

Moving bar of light evokes vectorial spatial selectivity in the immobile rat hippocampus

<https://doi.org/10.1038/s41586-022-04404-x>

Received: 1 May 2020

Accepted: 4 January 2022

Published online: 9 February 2022

 Check for updates

Chinmay S. Purandare^{1,2,5}, Shonali Dhingra^{1,5}, Rodrigo Rios¹, Cliff Vuong¹, Thuc To¹, Ayaka Hachisuka¹, Krishna Choudhary¹ & Mayank R. Mehta^{1,3,4}✉

Visual cortical neurons encode the position and motion direction of specific stimuli retrospectively, without any locomotion or task demand¹. The hippocampus, which is a part of the visual system, is hypothesized to require self-motion or a cognitive task to generate allocentric spatial selectivity that is scalar, abstract^{2,3} and prospective^{4–7}. Here we measured rodent hippocampal selectivity to a moving bar of light in a body-fixed rat to bridge these seeming disparities. About 70% of dorsal CA1 neurons showed stable activity modulation as a function of the angular position of the bar, independent of behaviour and rewards. One-third of tuned cells also encoded the direction of revolution. In other experiments, neurons encoded the distance of the bar, with preference for approaching motion. Collectively, these demonstrate visually evoked vectorial selectivity (VEVS). Unlike place cells, VEVS was retrospective. Changes in the visual stimulus or its predictability did not cause remapping but only caused gradual changes. Most VEVS-tuned neurons behaved like place cells during spatial exploration and the two selectivities were correlated. Thus, VEVS could form the basic building block of hippocampal activity. When combined with self-motion, reward or multisensory stimuli⁸, it can generate the complexity of prospective representations including allocentric space⁹, time^{10,11} and episodes¹².

Sensory cortical neurons generate selective responses to specific stimuli, in an egocentric (for example, retinotopic) coordinate frame, without any locomotion, memory or rewards¹. By contrast, the hippocampus is thought to contain a visually evoked, abstract, allocentric cognitive map, supported by spatially selective place cells², grid cells¹³ and head direction cells¹⁴. These responses are thought to arise from not only visual³ but also self-motion cues^{9,15}, for example, via path integration¹⁶. Recent studies have demonstrated hippocampal activity modulation by auditory^{17–19} or social stimuli^{20,21}. However, to elicit these responses, additional behavioural, cognitive or reward variables were required, whose removal nearly eliminated hippocampal selectivity^{17,18,22–25}. To our knowledge, no study has yet demonstrated hippocampal neural selectivity to a moving visual stimulus, without self-motion or rewards, similar to that found in visual cortices, even though they provide a major input to the hippocampus, and are thought to be crucial for hippocampal function. Hence, we investigated whether place cells encode the angular and linear position as well as motion direction of a simple stimulus, regardless of self-motion, memory or reward.

Rats were gently held in place on a large spherical treadmill, surrounded by a cylindrical screen²⁶. They could move their heads around the body by a small amount but could not turn their body. To keep them motivated, they were given random rewards, similar to typical place cell experiments, and were pretrained to do a virtual navigation task in the same apparatus (Methods). The only salient visual stimulus during the experiments was a vertical bar of light that was 74 cm tall, 7.5 cm wide and 33 cm away from

the rat, thus subtending a 13° solid angle. In the first set of experiments, the bar revolved around the rat at a constant speed (36° s⁻¹), without any change in shape or size (Fig. 1a, b). The revolution direction of the bar switched between clockwise (CW) and counterclockwise (CCW; or ‘anticlockwise’) every four revolutions. In subsequent experiments, we varied the colour, pattern, movement direction and trajectory of the bar. A majority of neurons showed selective responses in all cases.

Most CA1 neurons encode stimulus angle

We measured the activity of 1,191 putative pyramidal neurons (with a firing rate above 0.2 Hz during the experiment) from the dorsal CA1 of eight Long-Evans rats in 149 sessions using tetrodes (Methods)⁸. Many neurons showed clear modulation of firing rate as a function of the angular position of the bar, that is, angle VEVS (aVEVS) (Fig. 1c), with elevated firing rates in a limited region of visual angles. Across the ensemble of neurons, 464 (39%) showed significant (sparsity (z) > 2, corresponding to $P < 0.023$) (Methods, Extended Data Fig. 1) tuning in either the CW or CCW direction (Fig. 1d). These were classified as tuned cells, in contrast with untuned cells with $z < 2$.

Similar to the visual cortical neurons and hippocampal place cells, most tuning curves were unimodal (Extended Data Fig. 2) with a single preferred angle where the firing rate was the highest. Off responses (a significant decrease in firing rate) were virtually nonexistent. The preferred angles spanned the entire range, including angles behind the rat

¹W.M. Keck Center for Neurophysics, Department of Physics and Astronomy, UCLA, Los Angeles, CA, USA. ²Department of Bioengineering, UCLA, Los Angeles, CA, USA. ³Department of Neurology, UCLA, Los Angeles, CA, USA. ⁴Department of Electrical and Computer Engineering, UCLA, Los Angeles, CA, USA. ⁵These authors contributed equally: Chinmay S. Purandare, Shonali Dhingra. ✉e-mail: MayankMehta@ucla.edu

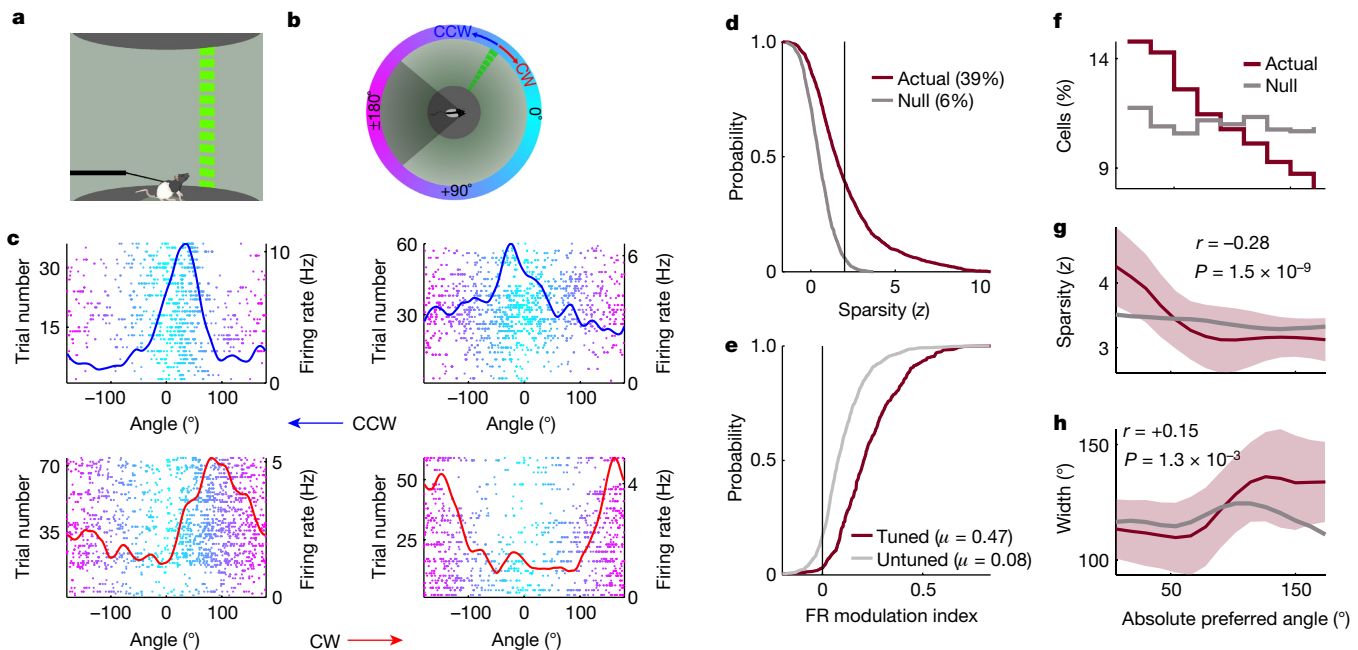


Fig. 1 | Hippocampal response to a revolving bar of light. **a, b**, Schematic of the experimental setup (**a**) and its top-down view (**b**). The field of view is 270° for the rat. The region behind the rat (dark grey) is invisible to him. CCW, counterclockwise; CW, clockwise. **c**, Trial number (y axis on the left) and firing rates (y axis on the right) of four CA1 neurons as a function of the angular position of the bar (front is 0°; behind is ±180°). Revolution direction of the bar: CCW is in blue (top); CW is in red (bottom). **d**, Cumulative distribution function of the strength of tuning (*z*-scored sparsity; Methods); response with higher tuning was chosen between CCW and CW (**d–f**). The measured data (maroon line) show significantly greater ($P = 1.26 \times 10^{-89}$, Kolmogorov–Smirnov test here

and in **e**) tuning than the shuffled data (grey line). 39% of neurons showed significant ($z > 2$) tuning. **e**, Cumulative distribution function of the firing rate (FR) modulation index within versus outside the preferred zone (Methods) for tuned cells ($z > 2$) was significantly different ($P = 1.9 \times 10^{-50}$) than untuned ($z < 2$) cells. **f**, Twice as many tuned cells (y axis) had their preferred angles (angle of maximal firing; x axis) in the front than behind. **g**, *z*-scored sparsity (the solid line is the median and the shaded area is the s.e.m. here and in **h**) of tuned cells decreased as a function of their preferred angle (Pearson correlation coefficient, here and in **h**, is also included). **h**, Full-width at quarter maxima of tuned responses increased with the preferred angle.

that he could not see barring rare occasions (Fig. 1f). These responses resembled striate cortical neurons in many ways^{1,27}. More neurons encoded the positions in front of the rat (0°) and there was a gradual twofold decline in the number of tuned cells for angles behind (±180°). The strength of aVEVS (Fig. 1g, Methods) was much larger near 0° than near 180°. The tuning curve width increased gradually (from 114° to 144°) (Fig. 1h) as a function of the absolute preferred angle from 0° to 180°. However, the widths were quite variable at every angle, spanning about one-third of the visual field, similar to place cells on linear tracks^{28,29}.

Hippocampal place cells on one-dimensional tracks have high firing rates within the field with little spiking outside²⁸. By contrast, most neurons with significant aVEVS spiked considerably outside the preferred zone, as evidenced by modest values of the firing rate modulation index (Fig. 1e, Methods). These broad aVEVS tuning curves resembled the angular tuning of CA1 neurons recently reported in the real world and in virtual reality³⁰, with a comparable fraction of neurons showing significant angular tuning. The trial-to-trial variability of aVEVS was comparable to recent experiments in visual cortex of mice under similar conditions³¹. Notably, the variability in the mean firing rate across trials was small and unrelated to the degree of aVEVS. However, the trial-to-trial variability of the preferred angle was quite large and predictive of the degree of aVEVS of a neuron (Extended Data Fig. 3).

Revolution direction selectivity of aVEVS

In the primary visual cortex, the majority of neurons respond selectively to the angular position of a stimulus, regardless of its movement direction¹. However, the majority of hippocampal neurons on linear tracks are directional, with far greater firing rate in one direction of journey^{8,28}. Furthermore, in both areas, neurons that are active in both directions, show significant and stable selectivity in both directions too. Hence, we

inspected the selectivity, directionality and stability (Methods) of the aVEVS. The firing rates were comparable for most neurons in two directions of revolution (see below). The degree of tuning varied continuously across neurons with no clear boundary between tuned and untuned neurons (Extended Data Fig. 4). Some neurons were bidirectional, that is, significant ($z > 2$) aVEVS in both directions of revolution (Fig. 2a, Extended Data Fig. 4). However, a larger subset of neurons was unidirectional, with significant ($z > 2$) aVEVS in only one movement direction (Fig. 2b, Extended Data Fig. 4). There were many untuned stable neurons, which were deemed untuned based on the standard, *z*-scored sparsity criteria ($z < 2$) but showed consistent, significantly stable (stability Kolmogorov–Smirnov test $P < 0.05$; Methods) spiking across trials (Fig. 2c, Extended Data Fig. 4). Across the ensemble, 13% (154) of neurons were bidirectional, 26% (310) were unidirectional, and the majority, 35% (421), were untuned stable (Fig. 2d, Extended Data Fig. 4). Thus, the vast majority (74%, 885) of hippocampal pyramidal neurons were consistently modulated by the angular position and direction of the revolving bar. However, unlike the visual cortex, far more aVEVS neurons were unidirectional, and unlike hippocampal place cells and the visual cortex, a far greater number of neurons showed untuned but stable responses. The preferred tuning angle was around 0°, that is, in front of the rat for most neurons (Extended Data Fig. 5), and this bias was greater for the bidirectional cells.

The highest (and significant) correlation between CCW and CW tuning curves was seen for bidirectional cells, followed by unidirectional cells and then untuned stable cells, but not for the untuned unstable cells (Extended Data Fig. 5). The mean rates were comparable in two directions, but were significantly larger in the direction with better aVEVS, largely because of an increase in firing within the preferred zone (±90° around the preferred angle) in the tuned direction. Higher rate cells were more likely to be bidirectional than unidirectional, even after accounting for the differences in firing rate (Extended Data Fig. 6).

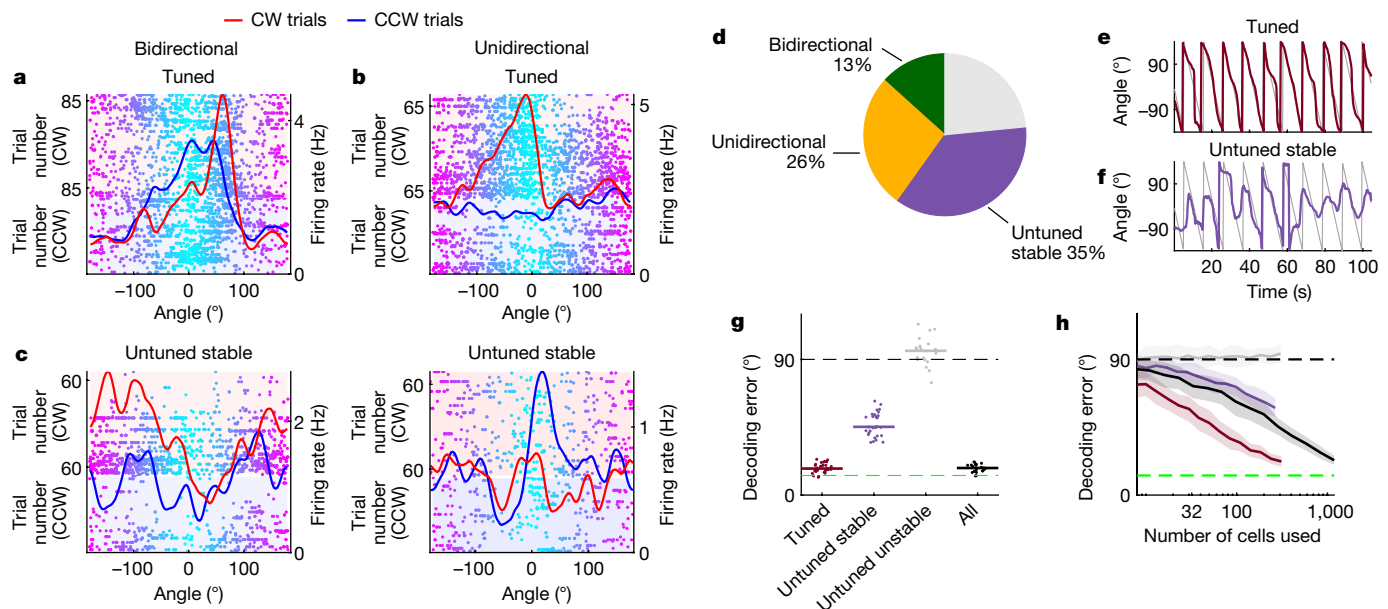


Fig. 2 | Directionality, stability and ensemble decoding of aVEVS.

a, A bidirectional cell, with significant ($z > 2$) tuning in both CCW and CW directions. **b**, Similar to **a**, but for a unidirectional cell, with significant tuning in only one direction (CW). **c**, Cells with multi-peaked, stable responses that did not have significant sparsity or tuning ($z < 2$) (bidirectional stable is shown on the left; unidirectional stable (CCW) is shown on the right). **d**, Distribution of selectivity. **e**, Decoded angle using only tuned cells in the CCW direction (maroon). **f**, Same as **e** but using only the untuned stable cells (lavender). **g**, Median error between stimulus angle and decoded angle over 30 instantiations

of 10 trials each for actual and shuffled data (not shown). The decoding errors for tuned ($\mu \pm \text{s.e.m.} = 17.6 \pm 0.6^\circ$) and untuned stable ($45.2 \pm 1.4^\circ$) were significantly less than that of shuffles (Kolmogorov–Smirnov test $P = 1.8 \times 10^{-14}$ for both). **h**, Decoding error (median $\pm \text{s.e.m.}$) decreases with increasing population size for all (black), tuned (maroon) and untuned stable (lavender) cells, but not for untuned unstable cells (grey). Grey shading denotes s.e.m. In **g** and **h**, the green dashed line indicates the width of the visual cue, and the black dashed line indicates the median error expected by chance.

Population vector decoding of aVEVS

In addition to individual cells, the population responses were also coherent for tuned and untuned stable populations (Methods, Extended Data Fig. 7). During spatial exploration, the ensemble of a few hundred place cells was sufficient to decode the position of the rat using population vector decoding³². Using similar methods, we decoded the angular position of the bar (Methods).

The ensemble of 310 tuned cells (CCW), with a short temporal window of 250 ms, could decode the angular position of the bar with a median accuracy of 17.6° (Fig. 2e, g), comparable to the bar width (13°) and similar to position decoding with place cells^{7,32}. In addition, the 266 untuned stable cells (CCW shown) could also decode the position of the bar significantly better than chance. Although the median error of 45.2° (Fig. 2f, g) was larger than that for the tuned cells, it was much smaller than chance (90°), further demonstrating significant aVEVS in untuned stable cells. Decoding performance improved when using a larger number of tuned or untuned stable cells (Fig. 2h). Thus the ensemble of untuned stable cells contained significant stimulus angle information, even though these individual cells did not³³. This was not the case for the untuned unstable cells.

aVEVS is retrospective

Under most conditions, visual cortical neurons respond to the stimulus with a short latency, that is, retrospectively, whereas most hippocampal bidirectional cells on linear tracks are prospective³, that is, they fire before the rat reaches a given position from the opposite movement directions^{6–8}. However, the converse was true for the bidirectional aVEVS (Extended Data Fig. 8). The preferred angle in the CCW direction lagged behind that in the CW direction (example cell) (Fig. 3c), that is, in both directions, the neuron responded to the bar after it had gone past a specific angle, which is a retrospective response. The circular difference

between the preferred angle between the CW and CCW directions (bidirectional population response) (Fig. 3a, b) was predominantly positive. We next asked whether only the peaks of aVEVS are retrospective or if the entire tuning curves show lagged responses. The cross-correlation between the entire tuning curves between the CW and CCW directions (Fig. 3d) of the majority (80%) of neurons showed maximum correlation at positive latency. Thus, most neurons responded to the moving bar retrospectively, that is, with a lag.

The median latency to response was 276.4 ms, which translates to a 19.9° median shift in cross-correlation (Fig. 3e). This retrospective coding was evident across the entire ensemble of bidirectional cells, such that the overlap of the population vector between the two directions was highest at values slightly above the diagonal (Fig. 3f, Methods).

Unidirectional cells also showed retrospective tuning, with a cross-correlation latency (19.9°, or 276.4 ms) comparable to bidirectional cells (Extended Data Fig. 9). Thus, the retrospective coding does not arise due to difference in tuning strengths. Small but significant retrospective bias was also observed in the untuned stable cells but not for the unstable cells (Extended Data Fig. 9). Additional experiments using a photodiode showed that this lag could not be explained by the latencies in the recording equipment (Extended Data Fig. 10).

Gradual change in aVEVS with stimuli and time

Change in distal visual cues causes remapping in place cells, that is, large changes in firing rate, degree of spatial selectivity and the preferred location^{34,35}. Conversely, primate hippocampal neurons show selectivity to a visual stimulus³⁶. To address this, we measured the responses of the same set of neurons, on the same day, to bars of light with gradual changes in their visual features (Methods), without any other changes. First, we changed the stimulus minimally (pattern change; row 1 in Fig. 3g, Fig. 3h–j). Neural firing rates, preferred tuning location and tuning curve profiles were largely invariant and comparable to intra-session

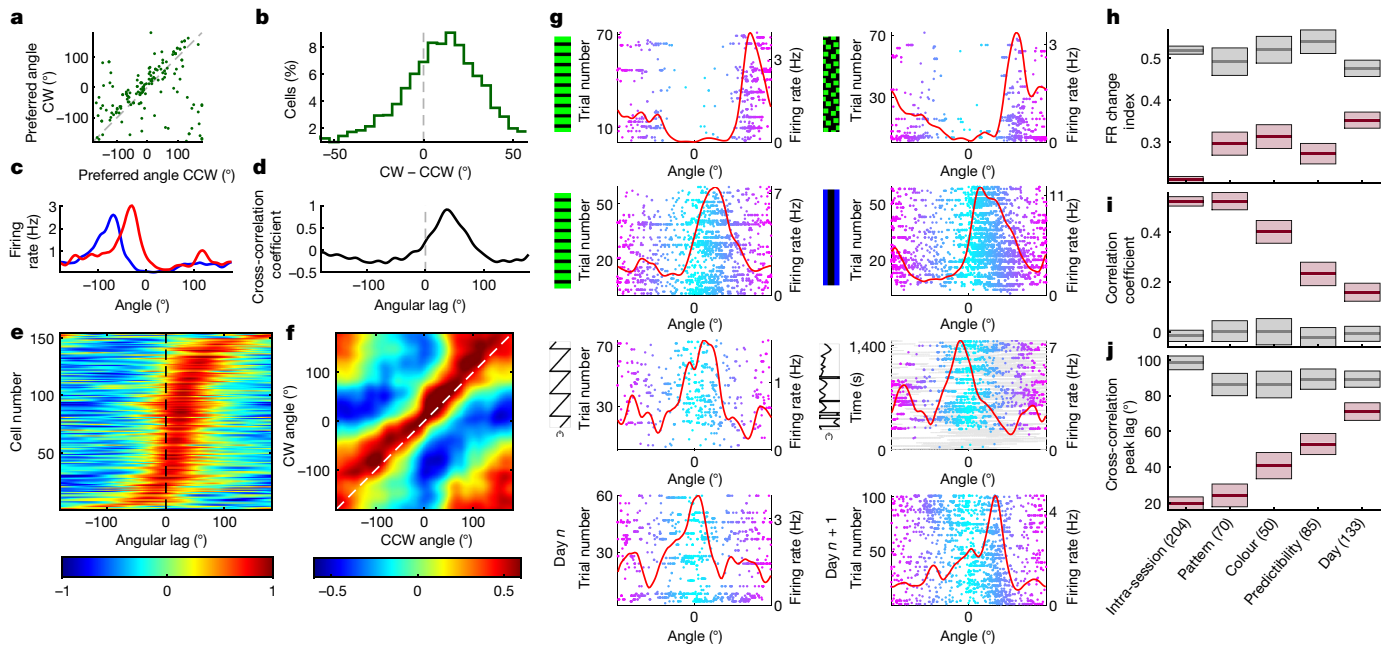


Fig. 3 | aVEVS is retrospective and changes gradually with stimulus pattern, colour, motion predictability and time. **a**, For bidirectional tuned cells, the preferred angle in the CW (y axis) direction was greater than that in the CCW (x axis) direction. **b**, Histogram of difference (CW – CCW, restricted to $\pm 50^\circ$) was significantly (t -test at 0° , $P = 0.003$) positive, indicating a retrospective shift. **c**, Retrospective latency between the CCW (blue) and CW (red) tuning curves for a bidirectional cell. **d**, Cross-correlation between the CW and CCW responses was maximum at positive latency ($+27^\circ$). **e**, Such cross-correlations were performed for each bidirectional cell and sorted according to their peak lag. The majority (80%) of lags were positive (median $+19.9 \pm 49.8^\circ$, circular median t -test at 0° , $P = 4.8 \times 10^{-16}$). **f**, Population vector overlap of aVEVS had a significant (circular median t -test, $P = 1.5 \times 10^{-36}$) peak at a positive lag (median $+54.3 \pm 25.3^\circ$). **g**, Change in pattern (green-striped (left) versus green-checkered (right)) caused the smallest change in aVEVS (row 1). Changes in colour (green versus blue; row 2) and pattern (horizontal versus vertical

stripes) caused gradually greater change in aVEVS. Changes in predictability of the stimulus motion (row 3) or mere passage of time (1 day) caused the greatest changes (row 4). Only CW example cells are shown here. **h**, Firing rate remapping, quantified by the firing rate change index, was significantly (Kolmogorov–Smirnov test, P value range 1.2×10^{-90} to 1.4×10^{-5}) smaller for the actual data (dark pink) than for the shuffled data (grey) for all conditions. **i**, Similar to **e**, the correlation coefficient between the tuning curves across different conditions was significantly greater than shuffle (Kolmogorov–Smirnov test P value range 2.6×10^{-58} to 3.8×10^{-6}). **j**, Same as **e**, the angular lag in cross-correlation to quantify the amount of shift between tuning curves across the two conditions. All were significantly lesser than shuffle (Kolmogorov–Smirnov test P value range 4×10^{-46} to 1.3×10^{-3}). n is shown in parentheses and indicates the number of responses measured. In **h–j**, the thick line indicates the median and the box represents the s.e.m.

variation (Fig. 3h–j, Methods). Next, we introduced larger change in the bar appearance by changing both colour and pattern. This resulted in significantly more changes in all measures of aVEVS, although this too was far less than expected by chance.

Sequential tasks can influence neural selectivity in the hippocampus^{9,10} and the visual cortex³⁷. Hippocampal neurons also show selectivity in sequential, non-spatial tasks^{19–21}. Sequential versus random goal-directed paths induce place field remapping in the real world³⁸ and large change in selectivity in virtual reality. To compute the contribution of the sequential movement of the bar of light to aVEVS, we designed a randomly moving bar paradigm (row 3 in Fig. 3g). The bar moved only 56.7° in one direction on average, and then abruptly changed speed and direction. This was called the ‘randomly’ moving bar experiment. Here, 26% of neurons showed significant aVEVS, which was far greater than chance, although lesser than the systematic condition (Extended Data Fig. 11). The percentage of unidirectional, bidirectional and untuned stable cells were qualitatively similar to the systematic stimulus experiments (Extended Data Fig. 11). Thus, the aVEVS cannot arise entirely from sequential movement of the bar. The retrospective latencies were also unaffected (Extended Data Fig. 9). To directly ascertain the effect of predictability on aVEVS, we separately analysed the randomly moving bar data in the first 1 s after flip of the stimulus direction, and an equivalent subsample of data from later (Methods, Extended Data Fig. 11). aVEVS was similar in these two conditions. Furthermore, aVEVS was not systematically biased by the angular movement speed of the stimulus, nor did hippocampal firing encode stimulus speed beyond chance levels (Extended Data Fig. 11).

Recent studies have reported representational drift, that is, slow remapping of place cells over several days³⁹. We measured the activity of the same cells for more than 1 day, and measured changes in aVEVS without any changes in stimuli for the predictably moving, systematic bar of light. There was a large remapping of aVEVS across 2 days, evidenced by a very low correlation between the tuning curves of the same neuron across 2 days (Fig. 3i). This was not due to difference in novelty, because rats had experienced this stimulus for at least 1 week.

Thus, unlike all-or-none changes in place cells that show complete remapping with large, but not small, changes in visual cues⁴⁰, aVEVS responses were largely invariant as measured by the correlation coefficient of the tuning curves (Fig. 3i). They showed gradually larger change in aVEVS with progressively greater changes in the visual cues, ranging from pattern, then colour, then predictability but largest with the passage of time. These results were partly mediated by the change in preferred angle under different conditions. However, even when this contribution was factored out, a similar pattern of changes was observed (Extended Data Fig. 11).

Most VEVS neurons are place cells

During spatial exploration, the majority of rodent hippocampal neurons show spatially selective responses, that is, place cells. Thus, we investigated the relationship between aVEVS and spatial selectivity of neurons. We measured the activity of the same set of CA1 neurons, on the same day, during the aVEVS protocol and while rats freely foraged

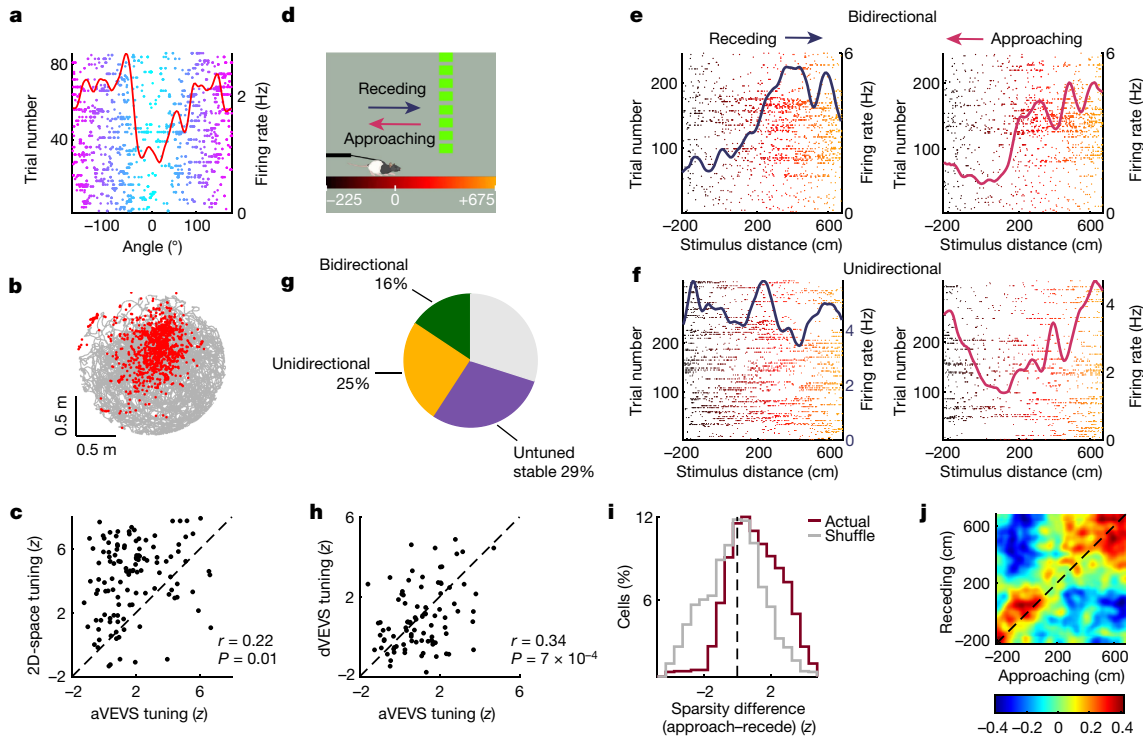


Fig. 4 | aVEVS cells are place cells and stimulus distance-encoding cells.

a, b. A cell recorded on the same day showing significant aVEVS in the revolving bar of the experiment (**a**) and allocentric spatial selectivity during free foraging on a circular table (**b**). The position of the rat (grey) and spikes (red) are shown. **c.** Strength of aVEVS and spatial selectivity measured by z-scored sparsity were significantly correlated (Pearson correlation is also indicated). **d.** Schematic of the stimulus distance experiment. The bar of light moved towards and away from the rat at a fixed angle (0°). **e.** Raster plots and firing rates of a bidirectional cell with significant tuning to the approaching (pink) as well as the receding (dark blue) bar of light. The trial number (y axis on the left) and firing rates (y axis on the right) are shown. **f.** Same as **e**, but for a unidirectional

cell, tuned for stimulus distance only during movement of the approaching stimulus. **g.** Relative percentages of cells, similar to Fig. 2d. **h.** Angular and linear stimulus distance tuning was positively correlated (Pearson correlation is also indicated). **i.** Stimulus distance tuning is larger during approaching epochs, even after down sampling spikes to have the same firing rate (Kolmogorov–Smirnov test actual $P = 4.6 \times 10^{-4}$, shuffle $P = 0.06$). **j.** Population vector overlap between responses in approaching and receding stimulus movement shows retrospective response, with maxima at values above the black diagonal dashed line, similar to Fig. 3f, corresponding to a median latency of 70.6 cm or 196.1 ms (± 377.6 ms).

for randomly scattered rewards in two-dimensional environments (Fig. 4a, b, Methods). Of the neurons that were active in the bar of light experiment, 79% (184 out of 234) were also active during spatial exploration. This is far greater than the fraction (approximately 20%) of place cells that are active in two different environments during spatial exploration. Furthermore, the firing rates during exploration and moving bar experiments were strongly correlated (Extended Data Fig. 12). Among cells that showed significant aVEVS, 90% (70 out of 78) showed significant spatial selectivity. Notably, the strength of tuning was also significantly correlated between these two experiments (Fig. 4c). Thus, despite very different experimental conditions and behaviour, the majority of aVEVS cells were also place cells, with similar activity and tuning.

Spatial exploration involves not only angular optic flow but also looming signals. Hence, in the same apparatus, we measured 147 cells when the stimulus moved towards or away from the rat, at a fixed angle of 0°, completing one lap in 10 s (Fig. 4d). Similar to the revolving bar experiments, the animal was body-restricted, and the movements of the rat had no effect on the motion of the bar or rewards (Fig. 1). The firing rates of 41% of neurons showed significant modulation as a function of the stimulus distance, that is, distance VEVS (dVEVS) (Fig. 4g), and 29% of cells had untuned but stable responses. Neurons not only encoded distance but also direction of movement, with 17% and 8% of neurons showing significant tuning to only the approaching (moving towards) or receding (moving away) bar of light, respectively. For cells recorded in both stimulus distance and angle experiments (Methods), firing rates (Extended Data Fig. 12) as well as the strength of tuning were correlated, suggesting that the same population of neurons can

encode both distance and angle (Fig. 4h). The preferred distance (that is, the position of maximal firing) for the bidirectional cells was not uniform but bimodal, with over-representation near the rat (0 cm) or the locations farthest away (500 cm) (Extended Data Fig. 12). Neural firing rates were quite similar for approaching and receding stimuli, but coding of the stimulus distance was much stronger for approaching movements (Fig. 4i). Retrospective response was also seen in distance VEVS (Fig. 4j), with the population overlap between approaching and receding responses shifted to values above the diagonal (Fig. 4j). This corresponds to a retrospective shift of 70.6 cm or 196.1 ms.

Discussion

These results demonstrate that a moving bar of light can reliably generate selectivity to distance, angle and direction of motion in hippocampal place cells, without any task demand, memory, reward contingency or locomotion requirements. Selectivity to these three spatial variables demonstrates VEVS, which is unlikely to arise due to non-specific variables (Extended Data Fig. 13 for reward-related controls, Extended Data Fig. 14 for behaviour-related controls, Extended Data Fig. 15 for generalized linear model estimates, Extended Data Fig. 16 for simultaneously recorded neurons showing diverse aVEVS and Extended Data Fig. 17 for quantification of co-fluctuation of firing responses). Similar to place cells, only a few hundred aVEVS neurons were sufficient to accurately decode the angular position of the stimulus. Positions in front of and near the rat were over-represented, similar to the visual cortices. The majority of neurons that encoded the bar position were also spatially selective during

Article

real-world exploration, and the strength of VEVS and spatial tuning were correlated. However, unlike place cells that shut down completely outside the place field, VEVS showed significant activity outside the preferred zone. Whereas place cells remap when the behaviour is sequential rather than random³⁸, aVEVS was relatively unchanged when the predictability or sequential nature of the stimuli was altered.

Whereas VEVS was retrospective, hippocampal place cells during spatial exploration^{5–8,41} and head direction cells in related areas^{42–44}, including in the virtual reality setup similar to that used here⁸, show prospective or predictive responses (Extended Data Fig. 8). Thus, self-motion signals may be required to turn the retrospective VEVS into prospective coding, necessary for navigational maps¹². Indeed, robust responses and prospective coding were seen in virtual reality, but for relative distance, not absolute position, as only the optic flow and locomotion cues were correlated at identical distance⁸.

These results show that during passive viewing, rodent hippocampal activity patterns fit the visual hierarchy⁴⁵. For example, aVEVS shows similar but smaller nasal-temporal magnification as the visual cortex, for example, a larger width of the tuning curve for more peripheral stimuli, and over-representation of the nasal compared with temporal positions²⁷. aVEVS is weaker but not absent for stimulus locations behind the rat, suggesting history dependence or other downstream processing providing stimulus information when it is not directly visible. History dependence could also explain the unidirectional responses in our experiments, also seen in the primary visual cortex⁴⁶, perhaps arising from similar plasticity mechanisms⁴⁷. Furthermore, similar to the visual cortex, hippocampal neurons too showed retrospective responses, but with larger response latency, suggesting that visual cortical inputs reached the hippocampus to generate VEVS. The larger latency is remarkably similar to that in the human hippocampus⁴⁸, and in the rodent cortico–entorhinal–hippocampal circuit during up–down states^{49–51}. However, there were no off responses in the VEVS and the tuning curves were broader and more unidirectional than in the primary visual cortex. This could arise due to processing in the cortico–hippocampal circuit, especially in the entorhinal cortex⁵¹, or due to the contribution of alternate pathways from the retina to the hippocampus⁵².

Hippocampal spatial maps are thought to rely on the visual cues³. Rats can not only navigate using only vision in virtual reality but they also preferentially rely on vision²⁶. Furthermore, rats can navigate in virtual reality without robust vestibular cues, and neurons show robust selectivity to distance travelled and the direction of the hidden reward location that predicts behavioural performance¹². Consistent with the multisensory pairing hypothesis^{9,30}, these multiplexed responses could arise when visual cue-evoked VEVS is paired with locomotion and reward cues during the navigation task. In the absence of any correlation between multisensory stimuli, hippocampal neurons generate invariant, non-abstract and retrospective VEVS, which are less robust than place cells. In real-world navigation tasks, the greatly enhanced correlations between all of the internal and external multisensory cues could be encoded more robustly via Hebbian plasticity to generate anticipatory or prospective coding of absolute position^{12,28,53}. Thus, the hippocampus can be driven reliably by a moving visual cue, similar to the visual cortex, to generate a vectorial representation of space in a polar coordinate frame centred on the head of the rat. When combined with self-motion, rewards and multisensory cues, this could elicit not only allocentric place cells² but also task-related hippocampal complexity¹².

Online content

Any methods, additional references, Nature Research reporting summaries, source data, extended data, supplementary information, acknowledgements, peer review information; details of author contributions and competing interests; and statements of data and code availability are available at <https://doi.org/10.1038/s41586-022-04404-x>.

- Hubel, D. H. & Wiesel, T. N. Receptive fields, binocular interaction and functional architecture in the cat's visual cortex. *J. Physiol.* **160**, 106–154 (1962).
- O'Keefe, J. & Dostrovsky, J. The hippocampus as a spatial map. Preliminary evidence from unit activity in the freely-moving rat. *Brain Res.* **34**, 171–175 (1971).
- O'Keefe, J. & Nadel, L. *The Hippocampus as a Cognitive Map* (Clarendon Press, 1978).
- Muller, R. U. & Kubie, J. L. The firing of hippocampal place cells predicts the future position of freely moving rats. *J. Neurosci.* **9**, 4101–4110 (1989).
- Mehta, M. R. Neuronal dynamics of predictive coding. *Neuroscience* **7**, 490–495 (2001).
- Battaglia, F. P., Sutherland, G. R. & McNaughton, B. L. Local sensory cues and place cell directionality: additional evidence of prospective coding in the hippocampus. *J. Neurosci.* **24**, 4541–4550 (2004).
- Resnik, E., McFarland, J. M., Sprengel, R., Sakmann, B. & Mehta, M. R. The effects of GluA1 deletion on the hippocampal population code for position. *J. Neurosci.* **32**, 8952–8968 (2012).
- Ravassard, P. et al. Multisensory control of hippocampal spatiotemporal selectivity. *Science* **340**, 1342–1346 (2013).
- Aghajan, Z. M. et al. Impaired spatial selectivity and intact phase precession in two-dimensional virtual reality. *Nat. Neurosci.* **18**, 121–128 (2015).
- Pastalkova, E., Itskov, V., Amarasingham, A., Buzsaki, G. & Buzsáki, G. Internally generated cell assembly sequences in the rat hippocampus. *Science* **321**, 1322–1327 (2008).
- MacDonald, C. J., Lepage, K. Q., Eden, U. T. & Eichenbaum, H. Hippocampal 'time cells' bridge the gap in memory for discontinuous events. *Neuron* **71**, 737–749 (2011).
- Moore, J. J., Cushman, J. D., Acharya, L., Popeney, B. & Mehta, M. R. Linking hippocampal multiplexed tuning, Hebbian plasticity and navigation. *Nature* **599**, 442–448 (2021).
- Fyhn, M., Molden, S., Witter, M. P., Moser, E. I. & Moser, M. B. Spatial representation in the entorhinal cortex. *Science* **305**, 1258–1264 (2004).
- Taube, J. S., Muller, R. U. & Ranck, J. B. Jr Head-direction cells recorded from the postsubiculum in freely moving rats. II. Effects of environmental manipulations. *J. Neurosci.* **10**, 436–447 (1990).
- Foster, T. C., Castro, C. A. & McNaughton, B. L. Spatial selectivity of rat hippocampal neurons: dependence on preparedness for movement. *Science* **244**, 1580–1582 (1989).
- McNaughton, B. L. et al. Deciphering the hippocampal polyglot: the hippocampus as a path integration system. *J. Exp. Biol.* **199**, 173–185 (1996).
- Sakurai, Y. Involvement of auditory cortical and hippocampal neurons in auditory working memory and reference memory in the rat. *J. Neurosci.* **14**, 2606–2623 (1994).
- Itskov, P. M. et al. Sound sensitivity of neurons in rat hippocampus during performance of a sound-guided task sound sensitivity of neurons in rat hippocampus during performance of a sound-guided task. *J. Neurophysiol.* **107**, 1822–1834 (2012).
- Aronov, D., Nevers, R. & Tank, D. W. Mapping of a non-spatial dimension by the hippocampal–entorhinal circuit. *Nature* **543**, 719–722 (2017).
- Omer, D. B., Maimon, S. R., Las, L. & Ulanovsky, N. Social place-cells in the bat hippocampus. *Science* **359**, 218–224 (2018).
- Danjo, T., Toyoizumi, T. & Fujisawa, S. Spatial representations of self and other in the hippocampus. *Science* **359**, 213–218 (2018).
- von Heimendahl, M., Rao, R. P. & Brecht, M. Weak and nondiscriminative responses to conspecifics in the rat hippocampus. *J. Neurosci.* **32**, 2129–2141 (2012).
- Mou, X. & Ji, D. Social observation enhances cross-environment activation of hippocampal place cell patterns. *eLife* **5**, 1–26 (2016).
- Dotson, N. M. & Yartsev, M. M. Nonlocal spatiotemporal representation in the hippocampus of freely flying bats. *Science* **373**, 242–247 (2021).
- Sakurai, Y. Coding of auditory temporal and pitch information by hippocampal individual cells and cell assemblies in the rat. *Neuroscience* **115**, 1153–1163 (2002).
- Cushman, J. D. et al. Multisensory control of multimodal behavior: do the legs know what the tongue is doing? *PLoS ONE* **8**, e80465 (2013).
- Malpeli, J. G. & Baker, F. H. The representation of the visual field in the lateral geniculate nucleus of *Macaca mulatta*. *J. Comp. Neurol.* **161**, 569–594 (1975).
- Mehta, M. R., Quirk, M. C. & Wilson, M. A. Experience-dependent asymmetric shape of hippocampal receptive fields. *Neuron* **25**, 707–715 (2000).
- Ahmed, O. J. & Mehta, M. R. The hippocampal rate code: anatomy, physiology and theory. *Trends Neurosci.* **32**, 329–338 (2009).
- Acharya, L., Aghajan, Z. M., Vuong, C., Moore, J. J. & Mehta, M. R. Causal influence of visual cues on hippocampal directional selectivity. *Cell* **164**, 197–207 (2016).
- de Vries, S. E. J. et al. A large-scale standardized physiological survey reveals functional organization of the mouse visual cortex. *Nat. Neurosci.* **23**, 138–151 (2020).
- Wilson, M. A. & McNaughton, B. L. Dynamics of the hippocampal ensemble code for space. *Science* **261**, 1055–1058 (1993).
- Stefanini, F. et al. A distributed neural code in the dentate gyrus and in CA1. *Neuron* **107**, 703–716.e4 (2020).
- Muller, R. U., Kubie, J. L., Bostock, E. M., Taube, J. S. & Quirk, G. J. in *Brain and Space* (ed. Paillard, J.) 296–333 (Oxford Univ. Press, 1991).
- Colgin, L. L., Moser, E. I. & Moser, M. B. Understanding memory through hippocampal remapping. *Trends Neurosci.* **31**, 469–477 (2008).
- Suzuki, W. A., Miller, E. K. & Desimone, R. Object and place memory in the macaque entorhinal cortex. *J. Neurophysiol.* **78**, 1062–1081 (1997).
- Saleem, A. B., Diamanti, E. M., Fournier, J., Harris, K. D. & Carandini, M. Coherent encoding of subjective spatial position in visual cortex and hippocampus. *Nature* **562**, 124–127 (2018).
- Markus, E. J. et al. Interactions between location and task affect the spatial and directional firing of hippocampal neurons. *J. Neurosci.* **15**, 7079–7094 (1995).
- Ziv, Y. et al. Long-term dynamics of CA1 hippocampal place codes. *Nat. Neurosci.* **16**, 264–266 (2013).
- Nakazawa, K. et al. Requirement for hippocampal CA3 NMDA receptors in associative memory recall. *Science* **297**, 211–218 (2002).
- Geiller, T., Fattahai, M., Choi, J.-S. S. & Royer, S. Place cells are more strongly tied to landmarks in deep than in superficial CA1. *Nat. Commun.* **8**, 14531 (2017).
- Taube, J. S. & Muller, R. U. Comparisons of head direction cell activity in the postsubiculum and anterior thalamus of freely moving rats. *Hippocampus* **8**, 87–108 (1998).

43. Deacon, T. W., Eichenbaum, H., Rosenberg, P. & Eckmann, K. W. Afferent connections of the perirhinal cortex in the rat. *J. Comp. Neurol.* **220**, 168–190 (1983).
44. Lozano, Y. R. et al. Retrosplenial and postsubiculum head direction cells compared during visual landmark discrimination. *Brain Neurosci. Adv.* **1**, 2398212817721859 (2017).
45. Felleman, D. J. & Van Essen, D. C. Distributed hierarchical processing in the primate cerebral cortex. *Cereb. Cortex* **1**, 1–47 (1991).
46. Hubel, D. H. & Wiesel, T. N. Receptive fields of single neurones in the cat's striate cortex. *J. Physiol.* **148**, 574–591 (1959).
47. Mehta, M. R. & Wilson, M. A. From hippocampus to V1: effect of LTP on spatio-temporal dynamics of receptive fields. *Neurocomputing* **32–33**, 905–911 (2000).
48. Quiroga, R. Q., Reddy, L., Kreiman, G., Koch, C. & Fried, I. Invariant visual representation by single neurons in the human brain. *Nature* **435**, 1102–1107 (2005).
49. Hahn, T. T., Sakmann, B. & Mehta, M. R. Phase-locking of hippocampal interneurons' membrane potential to neocortical up-down states. *Nat. Neurosci.* **9**, 1359–1361 (2006).
50. Hahn, T. T., Sakmann, B. & Mehta, M. R. Differential responses of hippocampal subfields to cortical up-down states. *Proc. Natl Acad. Sci. USA* **104**, 5169–5174 (2007).
51. Hahn, T. T. G., McFarland, J. M., Berberich, S., Sakmann, B. & Mehta, M. R. Spontaneous persistent activity in entorhinal cortex modulates cortico-hippocampal interaction in vivo. *Nat. Neurosci.* **15**, 1531–1538 (2012).
52. Beltramo, R. & Scanziani, M. A collicular visual cortex: neocortical space for an ancient midbrain visual structure. *Science* **363**, 64–69 (2019).
53. Mehta, M. R., Barnes, C. A. & McNaughton, B. L. Experience-dependent, asymmetric expansion of hippocampal place fields. *Proc. Natl Acad. Sci. USA* **94**, 8918–8921 (1997).

Publisher's note Springer Nature remains neutral with regard to jurisdictional claims in published maps and institutional affiliations.

© The Author(s), under exclusive licence to Springer Nature Limited 2022

Article

Methods

All experimental procedures were approved by the UCLA Chancellor's Animal Research Committee and were conducted in accordance with US federal guidelines.

Statistical tests

All usages of the Kolmogorov–Smirnov (KS) test were with two-sample, two-sided hypothesis testing. All Student's *t*-tests used were one-sample and used to test whether the distribution was centred at zero. Unless otherwise noted, correlation coefficients were computed as Pearson coefficients using the *corrcoef* function in MATLAB. Circular tests used to compare angular quantities in Fig. 3 and Extended Data Figs. 7 and 11 were executed with the *circ_stats* toolbox in MATLAB⁵⁴. Owing to the lack of multiple comparisons, no adjustments were necessary, except for the use of CCW as well as CW responses of the same cell in considerations of significantly tuned population.

Participants

Eight adult male Long-Evans rats (3 months old at the start of experiments) were individually housed on a 12-hour light–dark cycle. Their total food intake (15–20 g of food per day) and water intake (25–35 ml of water per day) were controlled and monitored to maintain body weight. Rats received 10–12 ml of water in a 20-min experiment. All experimental procedures were approved by the UCLA Chancellor's Animal Research Committee and were conducted in accordance with US federal guidelines.

Experimental apparatus

Rats were body restricted with a fabric harness as they ran on an air-levitated spherical treadmill of 30-cm radius. The rat was placed at the centre of a cylindrical screen with a radius of 33 cm and 74 cm high. Visual cues were projected on the screen. Although the rat was free to run and stop voluntarily, his running activity was decoupled from the projector and hence had no effect on the visual cues. Body restriction allowed the rat to scan his surroundings with neck movements. Running speed was measured by optical mice recording rotations of the spherical treadmill at 60 Hz. Head movement with respect to the harnessed and fixed body was recorded at 60 Hz using an overhead camera tracking two red LEDs attached to the cranial implant using the methods previously described⁸. Rewards were delivered at random intervals ($16.2\text{ s} \pm 7.5\text{ s}$, 2 rewards, 200 ms apart) to keep the rats motivated and the experimental conditions similar to typical place cell experiments.

Behavioural pre-training

All experiments were conducted in acoustically and EMF-shielded rooms. The rats were conditioned to associate a tone with a sugar-water reward. They were gently body-fixed in the apparatus that allowed them to move their heads with respect to the body, but the body could not turn around. For the rats to remain calm in the apparatus for long periods, they were trained to navigate in a visually rich virtual maze where a suspended, striped pillar indicated the rewarded position. After surgery, rats were exposed to the revolving bar environment for the first time, where the movement of the rat had no effect on the movement of the revolving bar. Six out of the eight rats never experienced virtual reality after the revolving bar experiments began.

Experiment design

The salient visual stimulus was a 13° wide vertical bar of light that revolved around the rat at a constant speed (10 s per revolution) without any change in shape or size (Fig. 1a). We used three different textures of visual cues as shown in Fig. 3. The results were qualitatively similar for all of the rats, hence the data were combined. Each block of trials consisted of four CW or four CCW revolutions of the bar of light. There were 13–15 blocks of trials in each session. During the random bar of light experiment, the bar revolved at one of the six speeds: ±36°, ±72°

or ±108° per second and spanning angles ranging 30–70° at any given speed, before changing the speed at random. Reward dispensing was similar to the systematic bar of light experiment, with no relation to the angular position or speed of the stimulus. Manipulations of stimulus colour, pattern, movement predictability and linearly moving stimulus were performed in a pseudo-random order in the same virtual reality apparatus. Real-world two-dimensional random foraging experiments and bar of light experiments were performed in a pseudo-random order, with an intermittent baseline of 25–40 min.

Surgery

All rats were implanted with 25–30 g custom-built hyperdrives containing up to 22 independently adjustable tetrodes (13-μm nichrome wires) positioned bilaterally over dorsal CA1 (−3.2 to −4.0 mm anterior–posterior, and ±1.75 to ±3.1 mm medial–lateral relative to bregma). Surgery was performed under isoflurane anaesthesia and heart rate, breathing rate and body temperature were continuously monitored. Two approximately 2 mm-diameter craniotomies were drilled using custom software and a CNC device with a precision of 25 μm in all three dimensions. Dura mater was manually removed and the hyperdrive was lowered until the cannulas were approximately 100 μm above the surface of the neocortex. The implant was anchored to the skull with 7–9 skull screws and dental cement. The occipital skull screws were used as ground for recording. Rats were administered approximately 5 mg per kg carprofen (Rimadyl bacon-flavoured pellets) 1 day before surgery and for at least 10 days during recovery.

Electrophysiology

The tetrodes were lowered gradually after surgery into the CA1 hippocampal subregion. Positioning of the electrodes in CA1 was confirmed through the presence of sharp-wave ripples during recordings. Signals from each tetrode were acquired by one of three 36-channel head stages, digitized at 40 kHz, band pass-filtered between 0.1 Hz and 9 kHz, and recorded continuously.

Spike sorting

Spikes were detected offline using a non-linear energy operator threshold, after application of a non-causal fourth-order Butterworth band pass filter (600–6,000 Hz). After detection, 1.5-ms spike waveforms were extracted. A custom-built 'PyClust' software was used for spike sorting as previously described⁸.

Tuning curves and z-score calculation

Procedures similar to that described previously were used⁸. We binned the angular occupancy of the vertical bar and spikes in $n = 120$ bins of width 3° each and smoothed it with a Gaussian of $\sigma = 12^\circ$. CW and CCW movement directions were treated separately. To quantify the degree of modulation, we computed sparsity s of an angular rate map where r_n is the firing rate in the n th angular bin:

$$s = 1 - \frac{1}{N} \frac{(\sum_n r_n)^2}{(\sum_n r_n^2)}$$

To assess the statistical significance of sparsity, we used a bootstrapping procedure, which does not assume a normal distribution. In brief, for each cell, in each movement direction, spike trains as a function of the vertical bar from each block of trials were circularly shifted by different angles and the sparsity of the randomized data was computed. This procedure was repeated 250 times with different sets of random value shifts. The mean value and standard deviation of the sparsity of randomized data were used to compute the z-scored sparsity of actual data using the function *zscore* in MATLAB. The observed sparsity was considered statistically significant if the z-scored sparsity of the observed spike train was greater than two, which corresponds to $P < 0.0228$ in a one-sided, Student's *t*-test.

A similar procedure was used for testing the significance angular tuning in the random bar of light condition. To keep the analysis comparable to the systematic condition, spike trains were circularly shifted with respect to behavioural data by different random amounts for each block of 40 s, which is comparable to the time taken by the systematic visual cue to undergo four revolutions.

In addition to sparsity, we quantified aVEVS using several other measures.

Direction selectivity index (DSI):

$$DSI = \frac{A_2}{A_2 + A_0}$$

where A_2 is the second harmonic component from the Fourier transform of the binned aVEVS response and A_0 is the mean level. This formulation of DSI is analogous to the orientation selectivity index (OSI), which is widely used in visual cortical selectivity quantification^{54–56}. 1- (circular variance) is equivalent to the mean resultant length (MVL) = $\sum_n r_n e^{i\theta_n}$ where r_n is the firing rate in the n th angular bin, θ_n is the angular position corresponding to this bin and n is summed over 120 bins.

Coherence (CH) = correlation coefficient($\{r_{n, \text{raw}}\}, \{r_{n, \text{smoothed}}\}$)

$$\text{Mutual information (MI)} = \sum_C p(C|\theta_n) \log_2 \frac{p(C|\theta_n)}{p(C)}$$

Where $P(C) = \sum_n P(\theta_n)P(C|\theta_n)$ and C is the average spike count in a 0.083-s window, which corresponds to 1 angular bin that is 3° wide. Statistical significance of these alternative measures of selectivity was computed similar to that for sparsity and is detailed in Extended Data Fig. 1.

Tuning curve width quantification

Full width at quarter maxima of the aVEVS rate map was computed around the maxima of the firing rate, that is, the preferred angle, as the width at which the tuning curve first crossed 0.25 times the peak value. We chose 0.25 of the maximum and not 0.5, that is, FWHM as commonly done, because the tuning curves are often very broad with non-zero activity at nearly all angles, which is missed by FWHM.

Modulation index calculation

The firing rate modulation index of the aVEVS (used in Fig. 1e) was quantified as $(FR_{\text{within}} - FR_{\text{outside}})/(FR_{\text{within}} + FR_{\text{outside}})$, where FR_{within} and FR_{outside} are average firing rates in their respective zones. Similar definition of the firing rate modulation index was used in Extended Data Fig. 5, to quantify the effect of unidirectional tuning inside and outside of the preferred zone, as $(FR_{\text{tuned}} - FR_{\text{untuned}})/(FR_{\text{tuned}} + FR_{\text{untuned}})$, where FR_{tuned} and FR_{untuned} are the average firing rates in the respective directions. Similarly in Extended Data Fig. 11, to quantify the effect of stimulus speed, as $(FR_{\text{fast}} - FR_{\text{slow}})/(FR_{\text{fast}} + FR_{\text{slow}})$, where FR_{fast} and FR_{slow} are the average firing rates during stationary epochs of respective stimulus movement speeds.

Spike train thinning

Neurons with a larger number of spikes, for example, due to longer experiments, have greater sparsity than when the number of spikes is less. To remove this artefact and compare the degree of aVEVS across all neurons and conditions, we used a spike thinning procedure. Randomly chosen spikes were removed such that the effective firing rate became 0.5 Hz for all neurons and then computed the sparsity of this thinned spike train (Extended Data Fig. 6). This procedure was used separately for CW and CCW directions to allow comparison of the degree of tuning in both directions, independent of the firing rate changes.

Stability analysis

The stability of neural angular tuning was quantified for CW and CCW directions separately. All the trials were split into two randomly chosen, equal and non-overlapping groups (approximately 30 trials each) and separate tuning curves computed for each half, with 120 equally spaced, non-overlapping angular bins. The correlation coefficient was computed between these two groups (C_{actual}), which is a measure of stability. To compute the significance of stability, this procedure was repeated 30 times, with different random grouping of trials, and the correlation coefficient computed between the two groups was computed each time. This provided a distribution of 30 values of stability C_{actual} . The same procedure was used for rate maps computed using random data (see z-score methods above) and the correlation computed between two groups to obtain 30 different values of C_{random} . The VEVs of a cell was considered significantly stable if the following conditions were met: the non-parametric rank-sum test comparing the 30 C_{actual} with 30 C_{random} was significant at $P < 0.05$ and $C_{\text{actual}} > C_{\text{random}}$. Untuned stable responses were identified as responses with significant stability, but non-significant tuning (sparsity (z) < 2), and were treated as a separate population in Fig. 2.

Population vector overlap

To evaluate the properties of a population of cells, sessions were divided into trials in the CCW and CW movement directions of the visual bar. Population vector overlap between CCW and CW movement direction at angles (θ_r, θ_m) for n single units was defined as the Pearson correlation coefficient between vectors $(\mu_{1,r}, \mu_{2,r}, \dots, \mu_{n,r})$ and $(\mu_{1,m}, \mu_{2,m}, \dots, \mu_{n,m})$ where $\mu_{i,p}$ is the normalized firing rate of the i th neuron at p th angular bin. Correlation coefficient of these sub-populations taken across angles indicates the existence of retrospective coding (Figs. 3f, 4j, Extended Data Fig. 9). Similarly, for computing coherence in either direction, population vector overlap between two groups of trials of the same bar movement direction (as defined above, in ‘Stability analysis’) was computed separately for CCW and CW trials (Extended Data Fig. 9). Populations of tuned, untuned but stable and untuned unstable cells were treated separately.

Decoding analysis

Using the stability labels as obtained from above, recorded cells were divided into three populations: tuned (sparsity $z > 2$), untuned (sparsity $z < 2$) and stable, untuned and unstable. All the trials across all the cells within each population were separated into two groups: ten, randomly chosen trials were treated as the ‘observed trials’ and this data were decoded using the firing rate maps obtained from the remaining trials or the ‘look-up trials’. A commonly used population vector overlap method was used between the look-up and observed trials using a window of 250 ms. In brief, at each 250-ms time point in the observed data, the correlation was computed between the observed population vector and the look-up population vectors at all angles. The circularly weighted average of angles, weighted by the (non-negative) correlations provided the decoded angle. The entire procedure was repeated 30 times for different sets of 10 trials. The error was computed as the circular difference between the decoded and actual angle at the observed time. Decoding of the stimulus distance (Extended Data Fig. 12) was done similarly but by finding the distance corresponding to maximum correlation between look-up and observed data, as circular averaging is unavailable for linear distance close to and away from the rat.

Same-cell identification

Spike sorting was performed separately for each session using custom software⁸. Identified single units were algorithmically matched between sessions to enable same-cell analysis (Figs. 3, 4). All of the isolated cells in one session were compared with all of the isolated cells in another session under investigation. Each putative unit pair was assigned a dissimilarity metric based on the Mahalanobis distance between their spike amplitudes, normalized by their mean amplitude. Dissimilarity

Article

numbers ranged from 2.5×10^{-5} to 17.2 across all combinations of units between two sessions. Putative matches were iteratively identified in an increasing order of dissimilarity, until this metric exceeded 0.04. These putative matches were further vetted, using an error index defined on their average spike waveforms.

Estimating the independent contribution of head position, running speed and stimulus angle using GLM

To compute the independent contributions of head position, running speed and stimulus angle, we used a generalized linear model (GLM)-based estimation of firing, using the `glmfit` function in MATLAB, as previously described³⁰. Head position and running speed were decoded in GLM using basis functions consisting of sinusoids. The log of running speed was used to ensure a similar amount of data in each bin, and bins with zero speed were assigned an arbitrary small value, which was on average equal to half the minimum non-zero running speed. Spike train and behavioural data were downsampled to 100-ms bins. The extreme one percentile of head position data and the top one percentile of running speed data were excluded to remove the effects of outliers and ensure a good fit. The CCW and CW tuning curves for stimulus angle were computed separately. The statistical significance of the resulting tuning curves was estimated by computing sparsity and a bootstrapping method described above and previously used³⁰.

Quantification of population remapping

To compute the amount of remapping of the firing rate, the strength of tuning, the preferred angle of firing and the similarity between CCW and CW aVEVS, we used the responses of the same cells recorded from different experimental conditions and defined remapping metrics as the firing rate modulation index, the difference between z-scored sparsity, the circular distance between the angles corresponding to maximal firing, the correlation coefficient between the firing rate profiles and the peak value and angular latency corresponding to the cross-correlation between their tuning curves in the two conditions. This calculation was repeated 100 times using a random permutation to break the same cell pairing, to obtain a null distribution. The mean and standard deviation of this distribution were plotted in Fig. 3h–j and Extended Data Fig. 11, and compared with the actual value of the corresponding remapping metric.

Quantification of trial-to-trial variability of aVEVS

Angular movement of the visual stimulus was separated into different trials starting and ending at 0°, which is the angular position in front of the rat. The mean firing rate in each trial was obtained by binning the spikes in that trial into 120 angular bins (3° wide), and finding the average value of firing rates in each bin. Similarly, the mean vector angle and the mean vector length were obtained using `circ_r` and `circ_mean` functions of the Circular Statistics toolbox in MATLAB⁵⁴ either by using all trials or only those trials when at least five spikes were recorded (each trial was 10 s long, yielding 0.5 Hz lowerbound on the mean firing rate).

Quantification of co-fluctuation for simultaneously recorded aVEVS

To determine whether the variability was correlated across simultaneously recorded tuned cells, a co-fluctuation index for firing rate

was defined for all cell pairs as the Spearman correlation between the trial-wise firing rate vectors of both cells. Co-fluctuation_{FR} = `spearman`($\{F_{1,k}\}, \{F_{2,k}\}$) where $F_{i,k}$ denotes the mean firing rate of i th cell on the k th trial. A bootstrapping procedure to access the significance of this index was used by obtaining 100 shuffled indices when the order of trials was randomly reassigned. Similarly, to estimate the co-fluctuation of aVEVS, we defined a similarity metric for each trial as $S_{i,k} = \text{crcf}(r_{n,k}, R_n)$ where n denotes the angular bins, R_n represents the overall tuning curve, and $r_{n,k}$ is the firing rate in the n th bin for the k th trial and `crcf` is the correlation coefficient function. Co-fluctuation of tuning was defined analogously as Co-fluctuation_{aVEVS} = `spearman`($\{S_{1,k}\}, \{S_{2,k}\}$), and bootstrapped similarly as the firing rate co-fluctuation index. Analogously, co-fluctuation of depth of modulation was quantified with the correlation coefficient of MVL as Co-fluctuation_{MVL} = `spearman`($\{L_{1,k}\}, \{L_{2,k}\}$), where $L_{i,k}$ denotes the MVL across stimulus angles of i th cell on the k th trial. Correlated changes in aVEVS preferred angle were quantified by Co-fluctuation_{MVA} = circular correlation($\{A_{1,k}\}, \{A_{2,k}\}$), where $A_{i,k}$ denotes the mean vector angle of spiking of i th cell on the k th trial.

Reporting summary

Further information on research design is available in the Nature Research Reporting Summary linked to this paper.

Data availability

The data that support the findings of this study are available from the corresponding author on reasonable request.

Code availability

All analyses were performed using custom-written code in MATLAB version R2016a. Codes necessary to reproduce the figures in this study are available from the corresponding authors upon reasonable request.

54. Berens, P. CircStat: a MATLAB toolbox for circular statistics. *J. Stat. Softw.* **31**, 1–21 (2009).
55. Ringach, D. L., Shapley, R. M. & Hawken, M. J. Orientation selectivity in macaque V1: diversity and laminar dependence. *J. Neurosci.* **22**, 5639–5651 (2002).
56. Ghodrati, M., Zavitz, E., Rosa, M. G. P. & Price, N. S. C. Contrast and luminance adaptation alter neuronal coding and perception of stimulus orientation. *Nat. Commun.* **10**, 941 (2019).

Acknowledgements We thank K. Delao, C. Polizu and S. Samant for help with data collection; V. Yuan, S. Ryklansky, A. Chorbajian and W. Zhu for help with single-unit clustering; and D. Dixit. This work was supported by grants to M.R.M. from the W.M. Keck Foundation, AT&T, NSF 1550678 and NIH 1U01MH115746.

Author contributions M.R.M. and C.S.P. designed the experiments. S.D., C.S.P., R.R., C.V., T.T., A.H. and K.C. performed the experiments. C.S.P. developed the stimuli and performed the analyses with input from M.R.M. M.R.M. and C.S.P. wrote the manuscript with critical input from S.D. and other authors.

Competing interests The authors declare no competing interests.

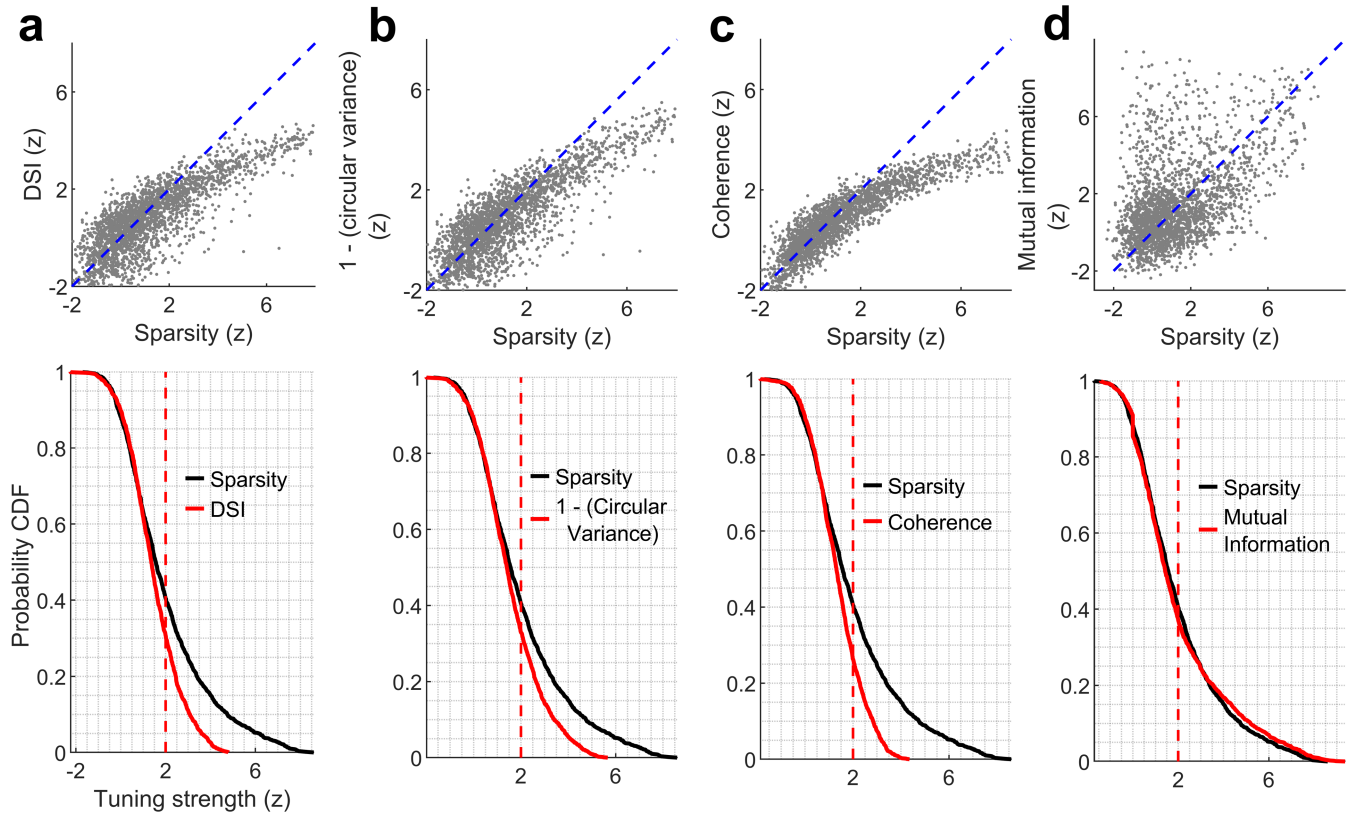
Additional information

Supplementary information The online version contains supplementary material available at <https://doi.org/10.1038/s41586-022-04404-x>.

Correspondence and requests for materials should be addressed to Mayank R. Mehta.

Peer review information *Nature* thanks the anonymous reviewers for their contribution to the peer review of this work. Peer reviewer reports are available.

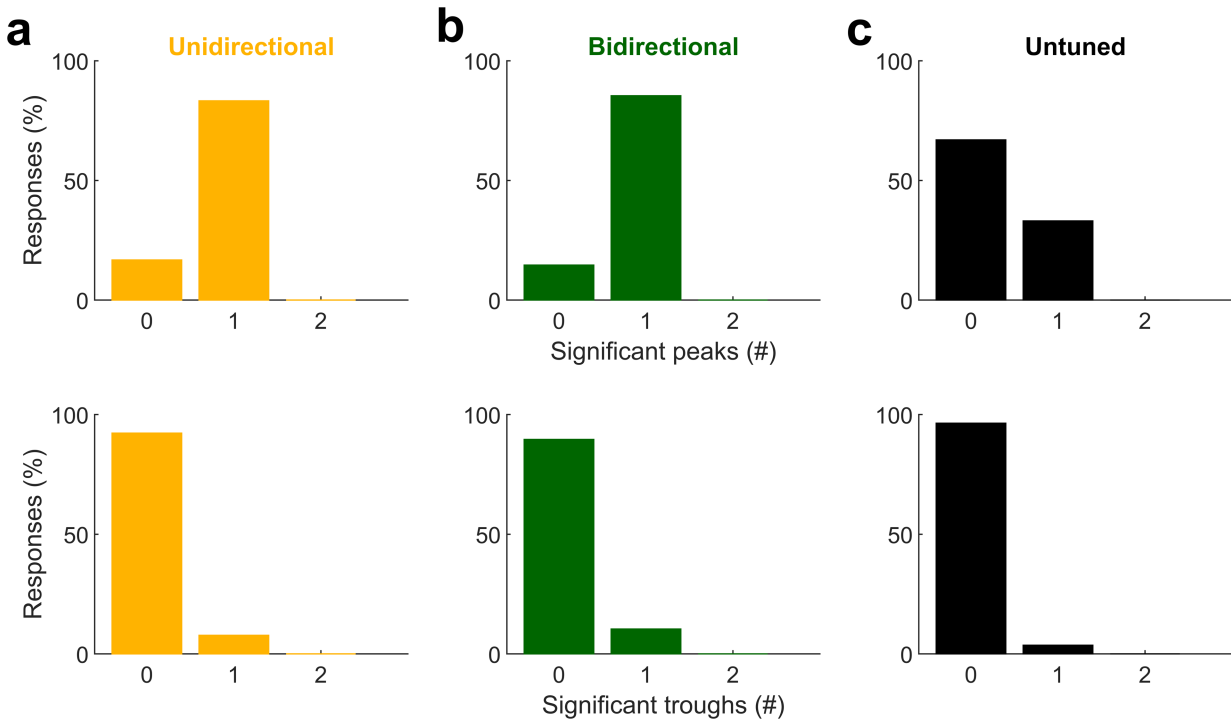
Reprints and permissions information is available at <http://www.nature.com/reprints>.



Extended Data Fig. 1 | Relationship between different properties of aVEVS.

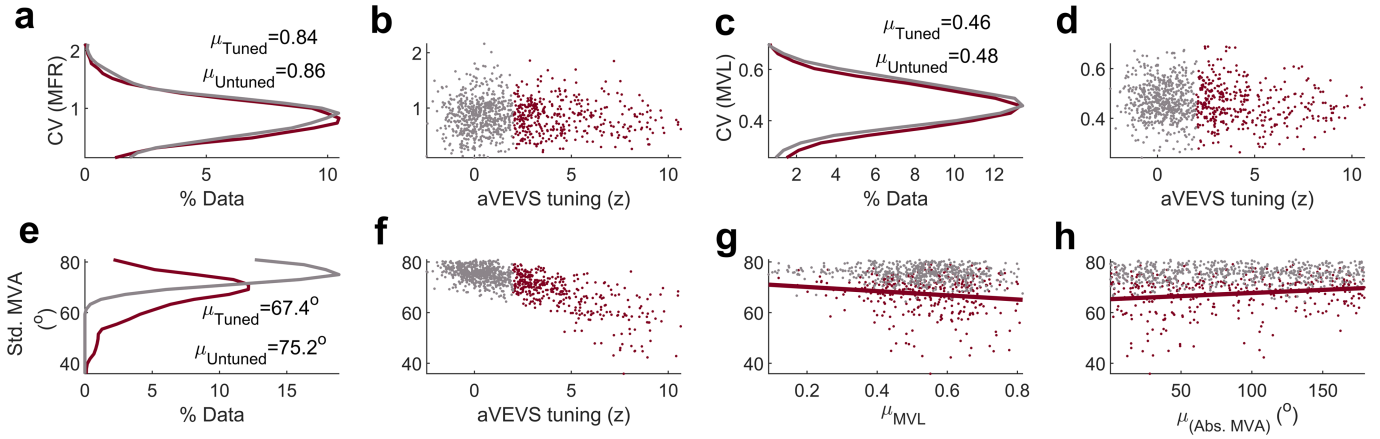
a, (top) aVEVS quantified by z-scored sparsity is significantly correlated ($r = 0.82, p < 10^{-150}$) with, but significantly greater than the z-scored direction selectivity index (DSI) (41% $z > 2$ for sparsity vs 31% for DSI, KS-test $p = 9.3 \times 10^{-10}$). (Bottom) Cumulative histogram (cdf) of z-scored metric of sparsity and DSI. **b,** Similar as **a**, (1 - (circular variance)) is significantly

correlated ($r = 0.84, p < 10^{-150}$) but significantly weaker (33% $z > 2$ for (1-circular variance)) than sparsity. (KS-test $p = 7 \times 10^{-6}$). **c,** Similar to **a** coherence is significantly correlated ($r = 0.89, p < 10^{-150}$) but significantly weaker (26% $z > 2$ for coherence KS-test $p = 6.3 \times 10^{-10}$) than sparsity. **d,** Similar to **a**, but mutual information is significantly correlated ($r = 0.47, p = 8.6 \times 10^{-132}$) but significantly smaller than sparsity (37% $z > 2$ for mutual information, KS-test $p = 7.2 \times 10^{-5}$).



Extended Data Fig. 2 | Unimodality of aVEVS. Majority of (a) uni-directional as well as (b) bi-directional tuning curves were unimodal with only one significant peak (top row), whereas (c) untuned responses did not have significant peaks, as expected. Both tuned responses were used for the bi-directional cells, and only the tuned response was used for the uni-directional cells. Significant troughs, i.e. off-responses were not found for unidirectional or bidirectional cells (bottom row). Significance of a peak (or

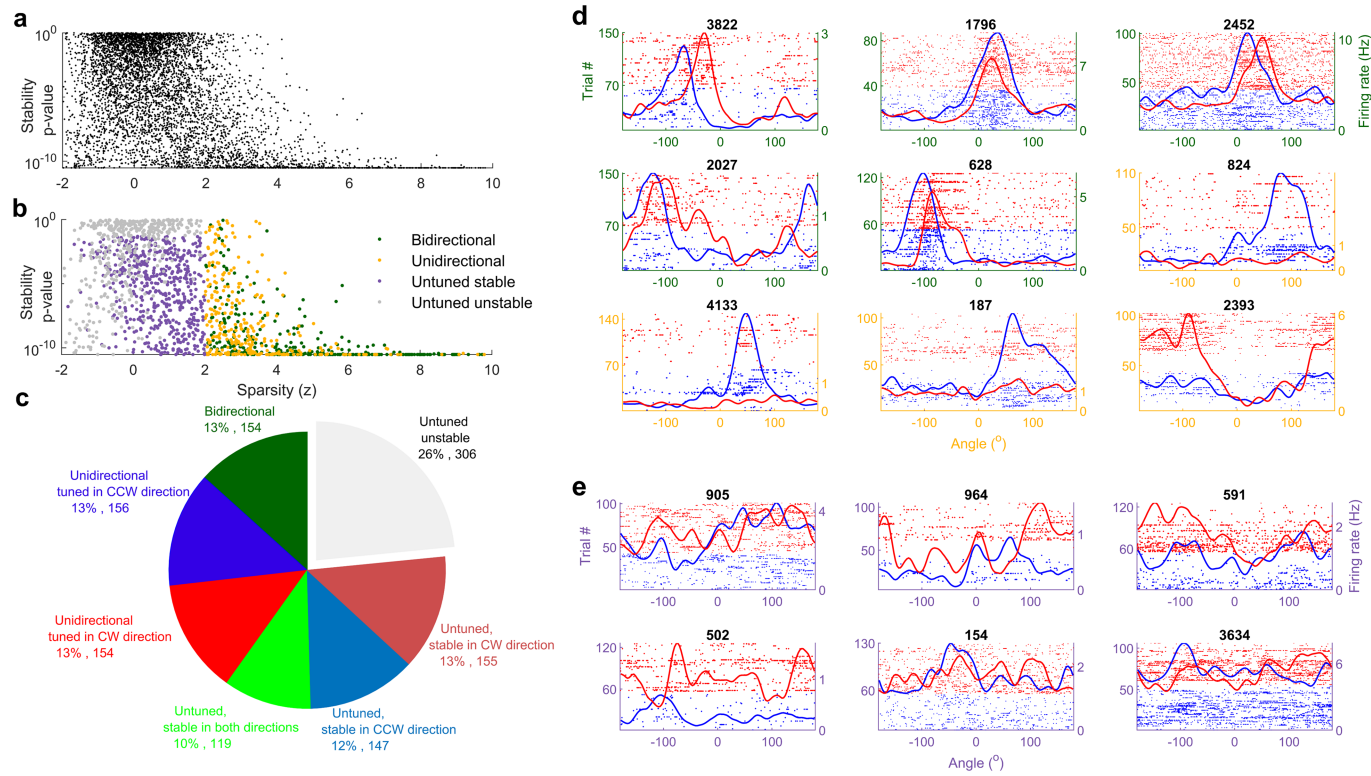
trough) was determined with the spike train shuffling analysis, similar to that performed to compute the z-scored sparsity. A peak (trough) was determined to be significant if it was larger (smaller) than the median value of peaks (troughs) in all shuffles and had a height of at least 20% of the range of firing rate variation in the shuffle data. These criteria resulted in zero significant peaks for some tuned responses.



Extended Data Fig. 3 | Trial-to-trial variability of mean vector angle but not mean firing rate determines aVEVS tuning. For each cell, in each trial, we computed the mean firing rate (MFR), mean vector length (MVL) and mean vector angle (MVA) of aVEVS (see Methods). To enable comparison across metrics, this analysis was restricted to responsive trials (firing rate above 0.5 Hz) where MVL and MVA could be meaningfully computed. Qualitatively similar results were obtained when this restriction was removed. **a**, Trial to trial fluctuations of firing rate was qualitatively similar between tuned (maroon) and untuned (gray) cells (KS-test $p = 0.25$). **b**, The variability was not significantly correlated with the degree of aVEVS tuning (Pearson partial correlation, after factoring out mean firing rate, $p = 0.85$). **c**, **d**, The variance of MVL (see Methods) was significantly greater for untuned cells (KS-test $p = 0.01$)

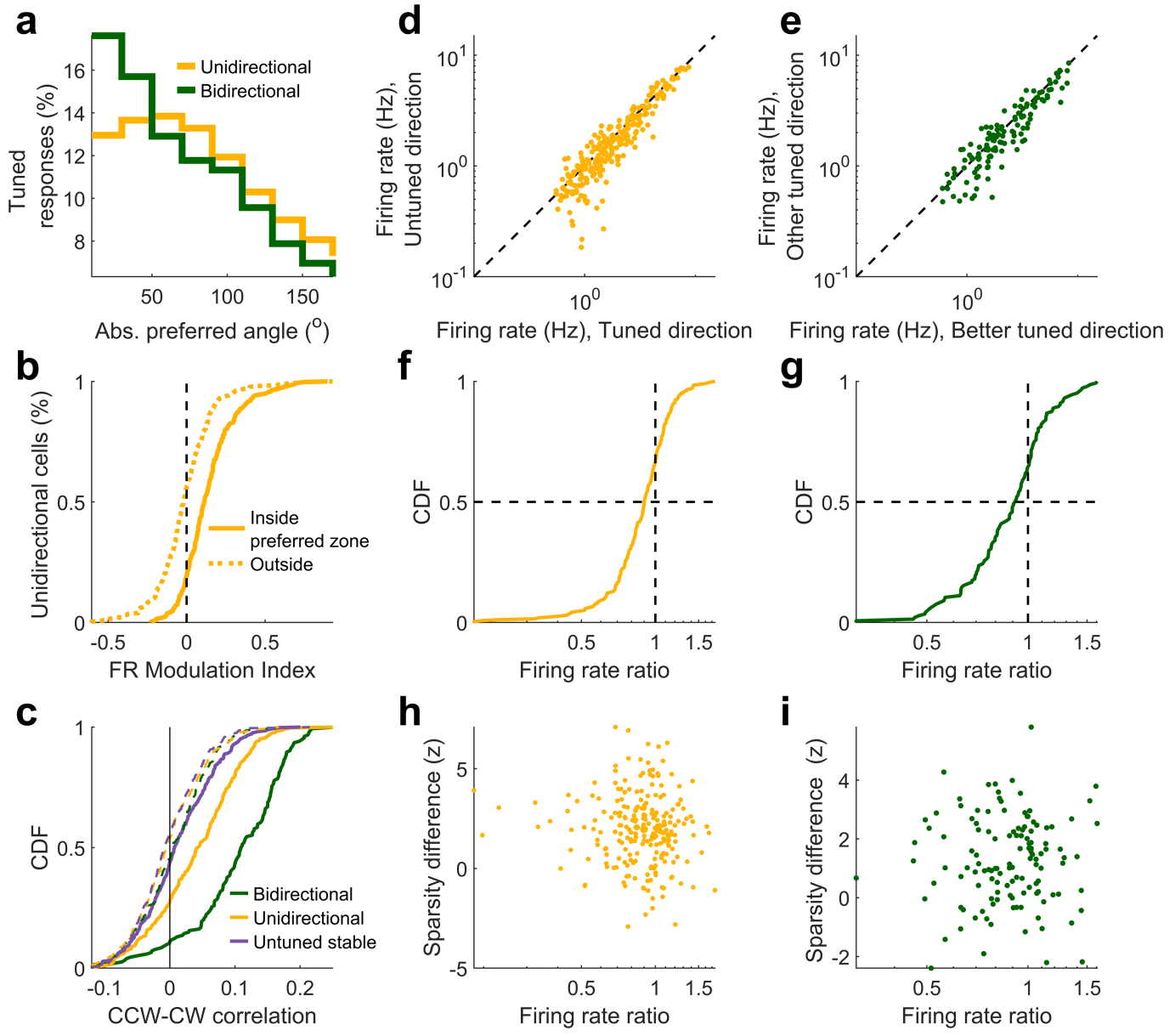
than tuned cells (**c**) and was inversely related to aVEVS tuning strength ($r = -0.19, p = 7.3 \times 10^{-10}$) (**d**). **e**, The circular standard deviation of MVA, which signifies the instability of aVEVS tuning from trial to trial, was significantly ($p = 1.3 \times 10^{-72}$) smaller (11%) for tuned than untuned cells and (**f**) strongly anti-correlated with aVEVS ($r = -0.77, p = 7.4 \times 10^{-192}$). **g**, This standard deviation of MVA was inversely correlated with MVL for tuned ($r = -0.15, p = 0.004$), and for untuned cells ($r = -0.12, p = 0.003$). **h**, It was also positively correlated with the preferred angle of tuning ($r = 0.18, p = 3.5 \times 10^{-4}$), with lower variability for cells tuned to the front angles (0°) than behind ($\pm 180^\circ$). Standard deviation of MVA was uncorrelated with preferred angle of tuning for untuned cells ($r = 0.02, p = 0.67$). All correlations were computed as Pearson correlation coefficients.

Article



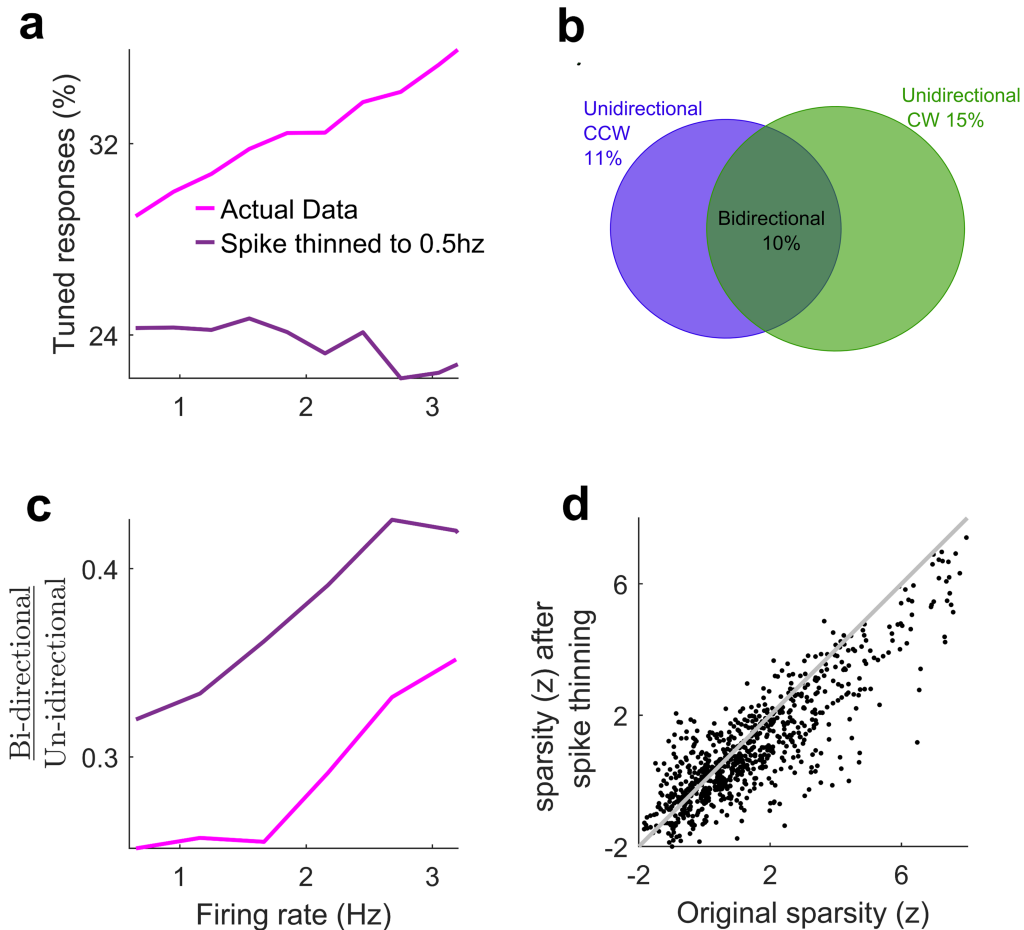
Extended Data Fig. 4 | Continuity of stability and sparsity measures and example cells. **a**, across all neurons, the z-scored sparsity, i.e., degree of tuning, and stability varied continuously, with no clear boundary between tuned and untuned neurons. **b**, Same distribution as **a**, with color-coding of stable and tuned responses separated. **c**, Detailed breakdown of aVEVS properties that had significant sparsity (i.e., tuned) or significant stability and whether these were observed in both directions (e.g., bidirectional stable) or only one direction (e.g. unidirectional tuned). If unidirectional, whether CW or

CCW direction was significant. Nearly all cells that were significantly tuned in a given direction were also stable in that direction. **d**, For clarity, the CCW (blue) and CW (red) trials are stacked separately in all raster plot figures, even though these alternated every four trials. First five examples are of bi-directionally tuned cells (green y-axis); next four examples are of uni-directionally tuned cells (orange-yellow y-axis). **e**, These cells did not have significant sparsity ($z < 2$) in either direction but had significant stability.



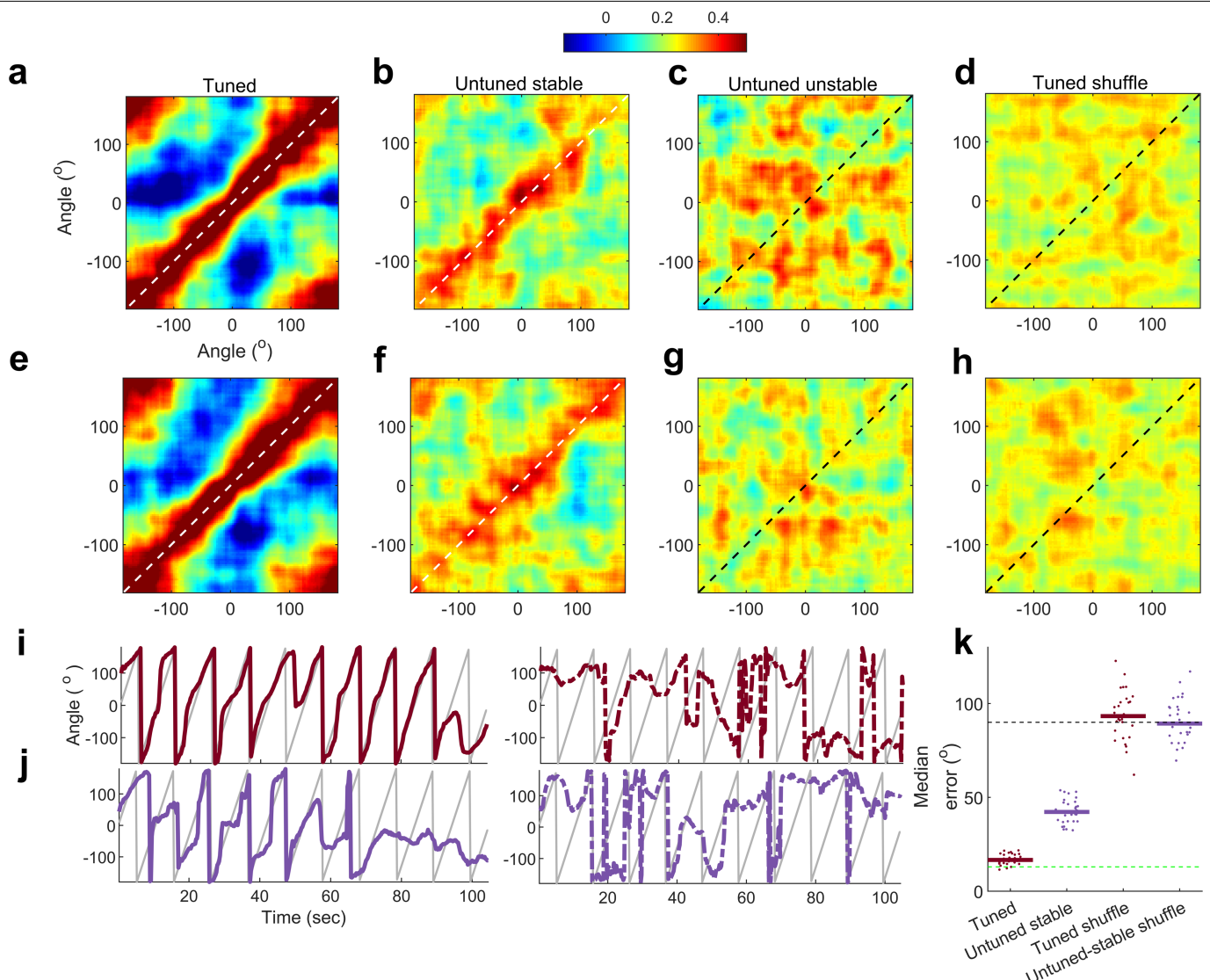
Extended Data Fig. 5 | Firing rate differences between CW and CCW revolution direction. **a**, Percentage of tuned responses as a function of the absolute preferred angle, for bidirectional and unidirectional populations are significantly different from each other (KS-test $p = 0.04$). **b**, Firing rate modulation index for uni-directional cells inside preferred zone was significantly different from zero (t-test, $p = 4.1 \times 10^{-35}$), but not outside ($p = 0.35$). **c**, Correlation coefficient of CCW and CW responses for different populations of cells, (KS-test green, bidirectional, $p = 3.3 \times 10^{-27}$, orange, unidirectional $p = 7.0 \times 10^{-27}$, lavender, untuned stable, $p = 4.4 \times 10^{-4}$). Dashed curves indicate respective shuffles. **d**, Firing rate of unidirectional cells in tuned versus untuned directions shows significantly higher (KS-test $p = 7.9 \times 10^{-9}$) firing rates in the tuned direction. **e**, Same as **d**, for bidirectional cells showing higher firing rate (KS-test, $p = 2.4 \times 10^{-18}$) in the revolution direction

with better tuning. **f**, Cumulative histogram of ratio between firing rate in untuned to tuned direction was less than one for 67% of cells. **g**, Same as **f**, but for bidirectional cells (other/better since both directions are tuned) showing 65% of firing rate ratios were less than one. **h**, To remove the contribution of firing rate to sparsity, the strength of tuning (z-scored sparsity) was computed with spike thinning procedures (similar to Extended Data Fig. 6; see Methods) ensuring equal firing rate in both directions. The difference in tuning strength (z-scored sparsity) was not significantly correlated with firing rate ratio for unidirectional ($r = -0.09 p = 0.16$) as well as **(i)** bidirectional ($r = 0.005 p = 0.95$) populations. For bi-directionally tuned cells, aVEVS with higher z-scored sparsity was labeled as the “better” response, and the aVEVS with lower z-scored sparsity was called “other” response. All correlations were computed as Pearson correlation coefficients.



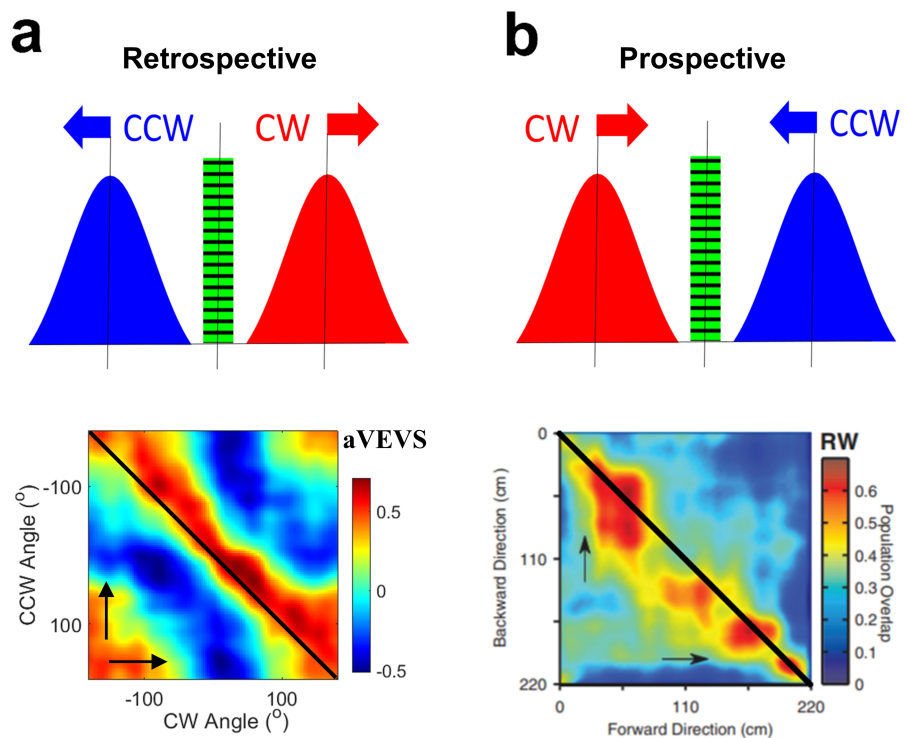
Extended Data Fig. 6 | The relative number of bidirectional cells increases with mean firing rate, but not the fraction of tuned cells. To remove the effect of firing rate on z-scored sparsity computation, we randomly subsampled spike trains to have a firing rate of 0.5 Hz (see Methods). **a**, The fraction of cells with significant sparsity, i.e., fraction tuned, increased with the firing rate for the actual data ($r = 0.11, p = 2.2 \times 10^{-6}$), but after spike thinning, there was no correlation ($r = 0.01, p = 0.77$). Thus, the true probability of being tuned was independent of the firing rate of neurons. **b**, Proportion of bidirectional and uni-directional tuned neurons is comparable (10% vs 13%)

with and without spike thinning. **c**, Fraction of bi-directional cells compared to uni-directional cells increases with original firing rate, even after spike train thinning. **d**, Spike thinning procedure reduces the sparsity of the tuning curves, as expected, due to loss of signal. After spike thinning, sparsity was significantly correlated in both directions of revolution ($r = 0.39, p = 3.8 \times 10^{-31}$) and this was not due to the rate changes because sparsity was uncorrelated with firing rates ($r = 0.01, p = 0.72$ for CCW sparsity and firing rate, $r = 0.02, p = 0.54$ for CW sparsity and firing rate). All correlations were computed as Pearson correlation coefficients.



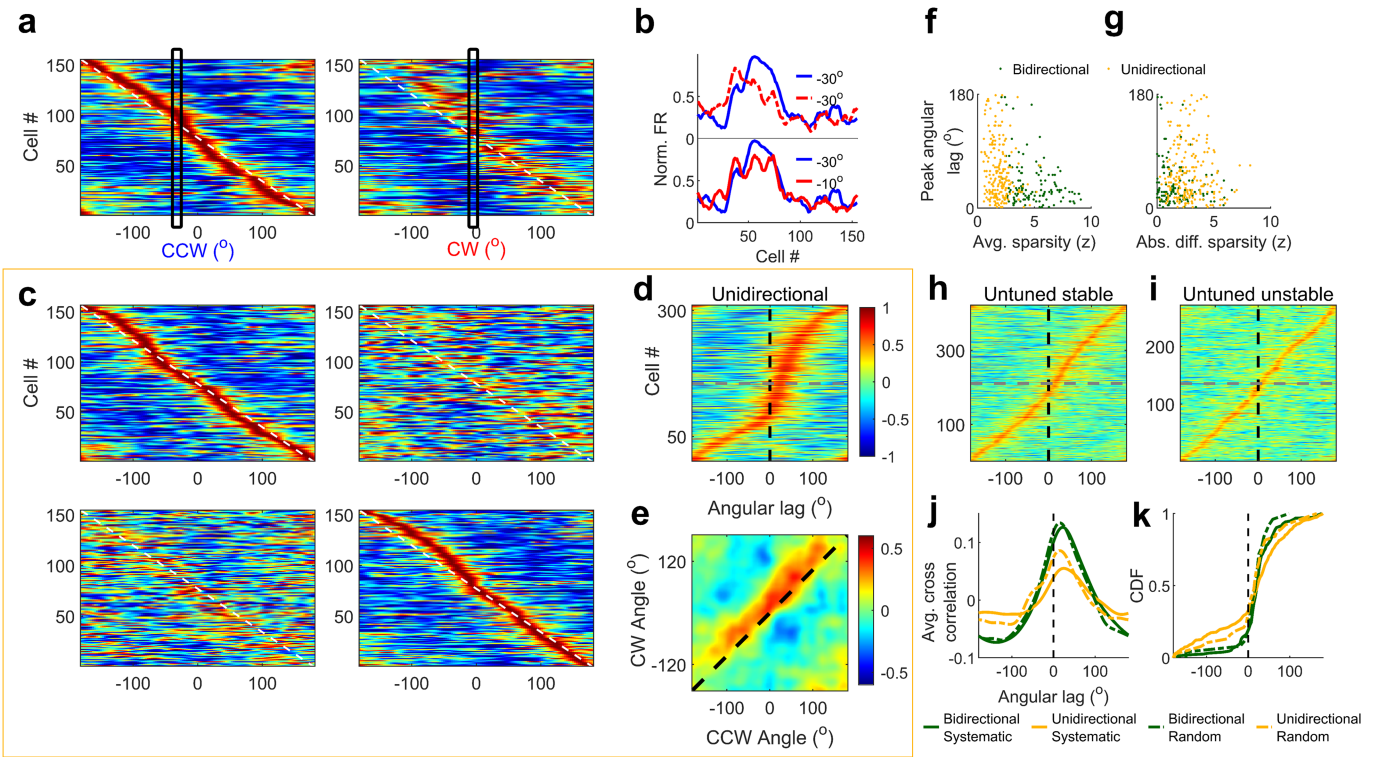
Extended Data Fig. 7 | Population vector stability and decoding of visual cue angle. **a**, Stability for CCW tuned responses (number of cells, $n = 310$). Color indicates correlation coefficient between two non-overlapping groups of trials' population responses (see Methods). The maximum correlation values were pre-dominantly along the diagonal. Maxima along x-axis and y-axis were significantly correlated (Circular correlation coefficient $r = 0.97$, $p < 10^{-150}$). **b**, Same as **a** but using untuned stable cells ($n = 266$) showed significant ensemble stability ($r = 0.91$, $p < 10^{-150}$). **c**, Same as **a** but using untuned and unstable cells ($n = 306$). This was not significantly different than chance ($r = -0.16$, $p = 0.09$). **d**, Same as **a**, using tuned cells with their spike trains circularly shifted in blocks of four trials, showed no significant stability ($r = 1.1 \times 10^{-3}$, $p = 0.99$). **e–h**, Same as **a–d**, but for CW data. **i**, Decoding CW direction shows similar results as in CCW direction (shown earlier in Fig. 2). Similar analysis as shown in Fig. 2 for the stimulus movement in CW direction. (Left) Decoding cue angle in 10 trials of CW cue movement, using all other CW trials to build a population-encoding matrix. Gray trace indices movement of visual bar, colored trace is the decoded angle. (Right) Same as left, for shuffle data. **j**, Same as **i** but using the untuned-stable cells in CW movement direction. **k**, Median error between stimulus angle and decoded angle over 10 instantiations of decoding 10 trials each for actual and cell ID shuffle data. Green dashed line indicates width of the visual cue; black dashed line indicates median error expected by chance.

($r = 1.1 \times 10^{-3}$, $p = 0.99$). **e–h**, Same as **a–d**, but for CW data. **i**, Decoding CW direction shows similar results as in CCW direction (shown earlier in Fig. 2). Similar analysis as shown in Fig. 2 for the stimulus movement in CW direction. (Left) Decoding cue angle in 10 trials of CW cue movement, using all other CW trials to build a population-encoding matrix. Gray trace indices movement of visual bar, colored trace is the decoded angle. (Right) Same as left, for shuffle data. **j**, Same as **i** but using the untuned-stable cells in CW movement direction. **k**, Median error between stimulus angle and decoded angle over 10 instantiations of decoding 10 trials each for actual and cell ID shuffle data. Green dashed line indicates width of the visual cue; black dashed line indicates median error expected by chance.



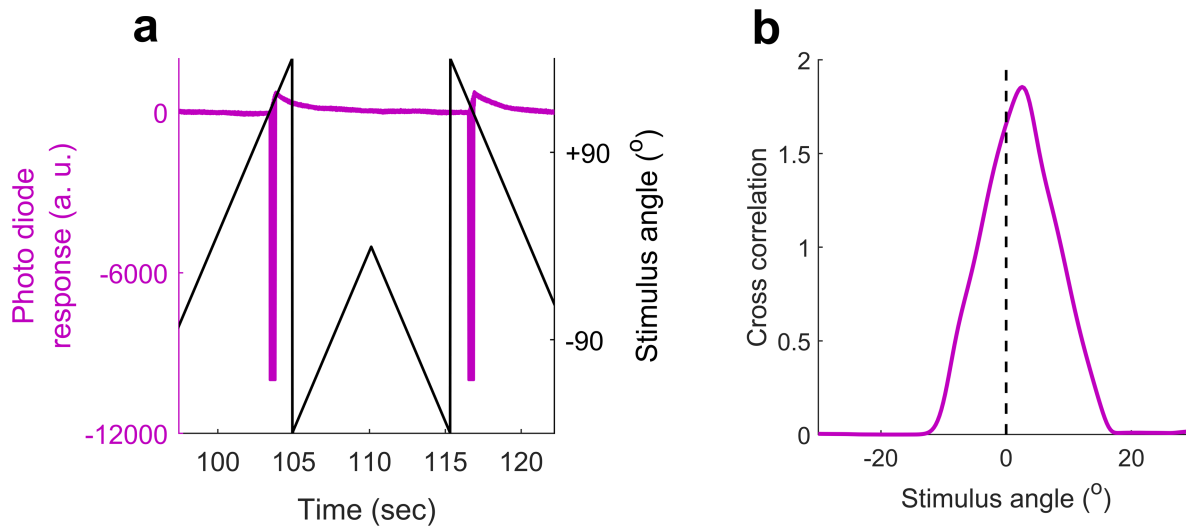
Extended Data Fig. 8 | Retrospective coding of aVEVS cells versus prospective coding in place cells. **a**, (Top) A bidirectional cell responds with a latency after the stimulus goes past the angular position of the bar of light depicted by the green striped bar. (Bottom) Population overlap is above the 45° line, indicating retrospective response. **b**, Same as **a** but for a prospective response, where the neuron responds before the stimulus arrives in the

receptive field. Such prospective responses are seen in place fields during navigation in the real world, where the population overlap is maximal below the 45° line (adapted from earlier work⁸). Prospective coding was seen in purely visual virtual reality, but those cells encoded prospective distance, not position.



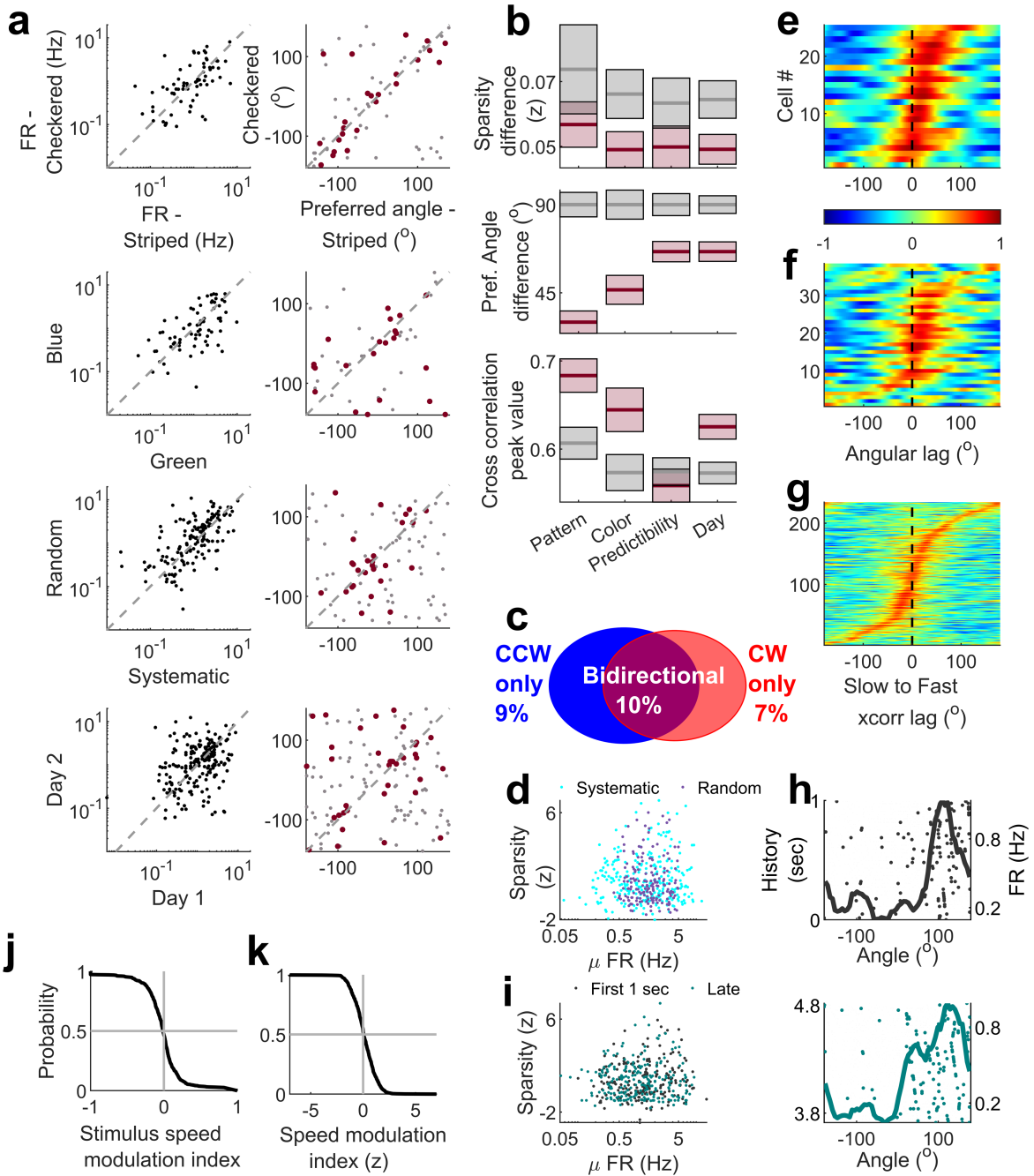
Extended Data Fig. 9 | Significant retrospective aVEVS in the unidirectional and untuned stable cells but not unstable cells. **a**, Stack plots of normalized population responses of cells, sorted according to the peak angle in the CCW (left). The corresponding responses of cells in the CW direction (right). **b**, The firing rate, averaged across the entire ensemble of bidirectional cells at -30° in the CCW direction was misaligned with the same in CW direction at the same angle (top), but better aligned with the response at -10° (bottom, vertical boxed in **a**), showing retrospective response. **c**, Same as **a** for uni-directional cells with CCW tuned cells (top row) and CW tuned cells (bottom row) sorted according to their aVEVS peak in the tuned direction. **d**, Same as in Fig. 3e for unidirectional cells. Majority (67%) of the cross correlations between CW and CCW responses had a significantly positive lag (median latency = $19.9^\circ \pm 86.1^\circ$, circular median t-test at 0° , $p = 1.8 \times 10^{-10}$). The larger range of latencies and weaker correlations for unidirectional cells compared to the bidirectional cells could arise because significant tuning is present in only one direction. **e**, Same as Fig. 3f for unidirectional cells. For all angles the population vector cross correlation coefficients had a peak at a positive lag (CW peak–CCW peak, median = $+56.2^\circ \pm 23.7^\circ$ circular median t-test, $p = 1.5 \times 10^{-36}$), which was not significantly different from the retrospective lag in bidirectional cells (KS-test, $p = 0.28$). **f**, Average strength of tuning in CCW and CW direction is inversely related to the peak angular lag between the two aVEVS for bidirectional

(Pearson's $r = -0.19 p = 0.04$) as well as unidirectional cells (Pearson's $r = -0.16 p = 0.02$). **g**, Absolute difference between strengths of tuning between CCW and CW directions was not significantly correlated with the peak angular lag in their cross correlation for bidirectional ($r = 0.13 p = 0.14$) or unidirectional cells ($r = 0.03 p = 0.64$). This analysis was restricted to cells with retrospective lags, which were in majority. **h**, Untuned stable cells too show significant retrospective bias, quantified using the cross correlation between the tuning curves in CCW and CW directions (median lag = 13.6° circular median t-test at 0° , $p = 0.02$). **i**, This is not seen for the untuned unstable population (median = 4.6° , circular median t-test at 0° , $p = 0.39$). **j**, Cross-correlations between CCW and CW tuning curves were averaged across all the bidirectional cells (green curves) for the systematic (latency for peak = 25.7°) and random (16.7°) condition and showed a similar pattern of retrospective coding. (two sample KS-Test to ascertain if the distribution of latencies was significantly different, $p = 0.75$). Unidirectional cells showed similar pattern for systematic (19.7°) and random (31.8°) conditions, but correlations were weaker than bidirectional cells. **k**, Cumulative distributions show that under systematic and random conditions comparable number of cells had positive latency (80% each) for bidirectional cells, and (67% and 68%) unidirectional cells respectively.



Extended Data Fig. 10 | Photodiode experiment to measure the latency introduced by the equipment. Instead of a rat, we placed a photodiode where the rat sat. **a, b**, The signal from the photodiode (purple trace) synchronized with bar position (black) was extracted (**a**) and cross correlation computed between the CW and CCW tuning curves of photodiode response (**b**). The cross correlation had maxima at a latency of -2.8° , which corresponds to a temporal

lag of 38.9 ms. This was much smaller than the latency between neural spike trains (median latency 22.7° , corresponding to a temporal latency of 315.3 ms before accounting for the recording apparatus latency). For all the latency numbers reported in the main text, this small latency introduced by the recording apparatus was removed.

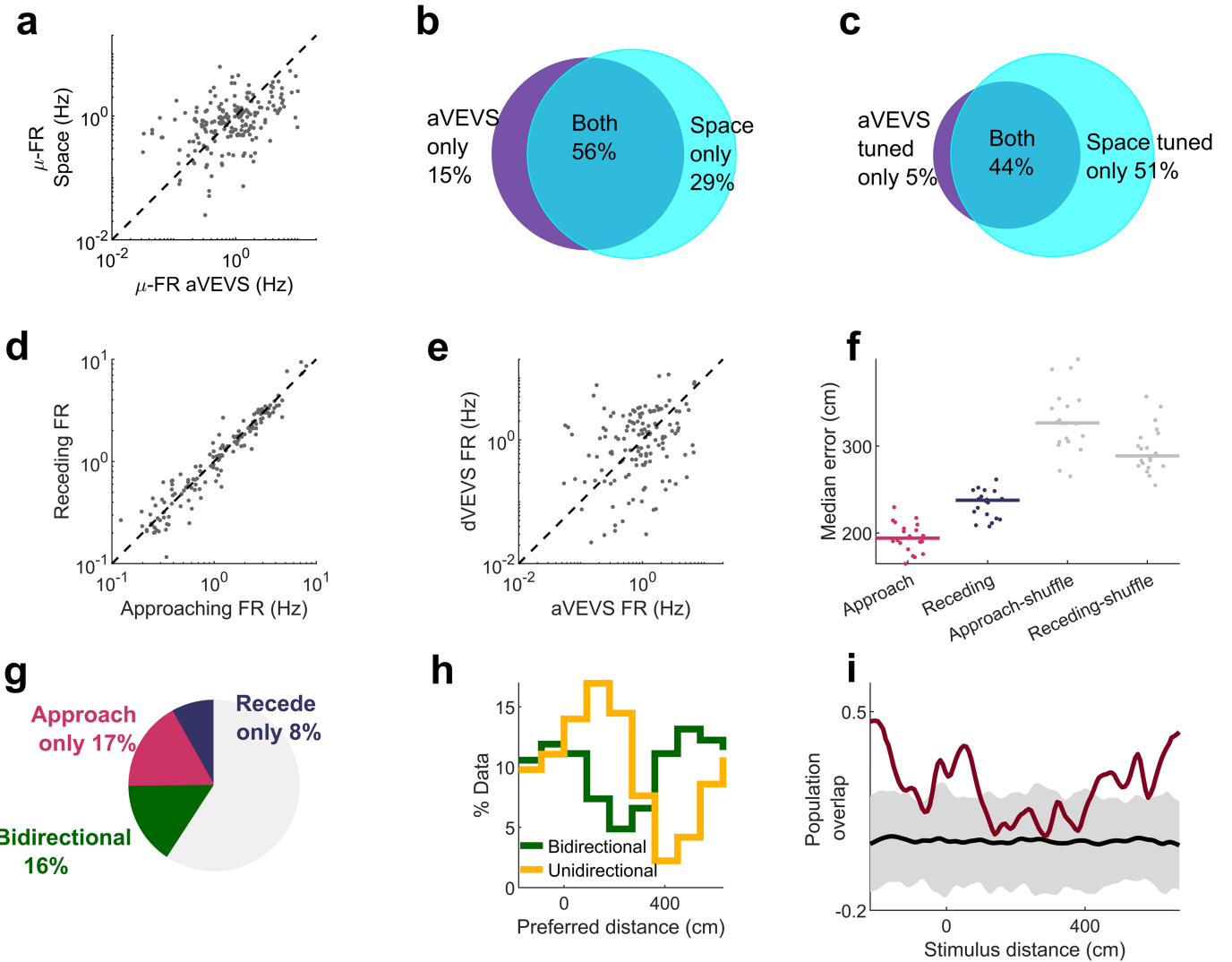


Extended Data Fig. 11 | See next page for caption.

Article

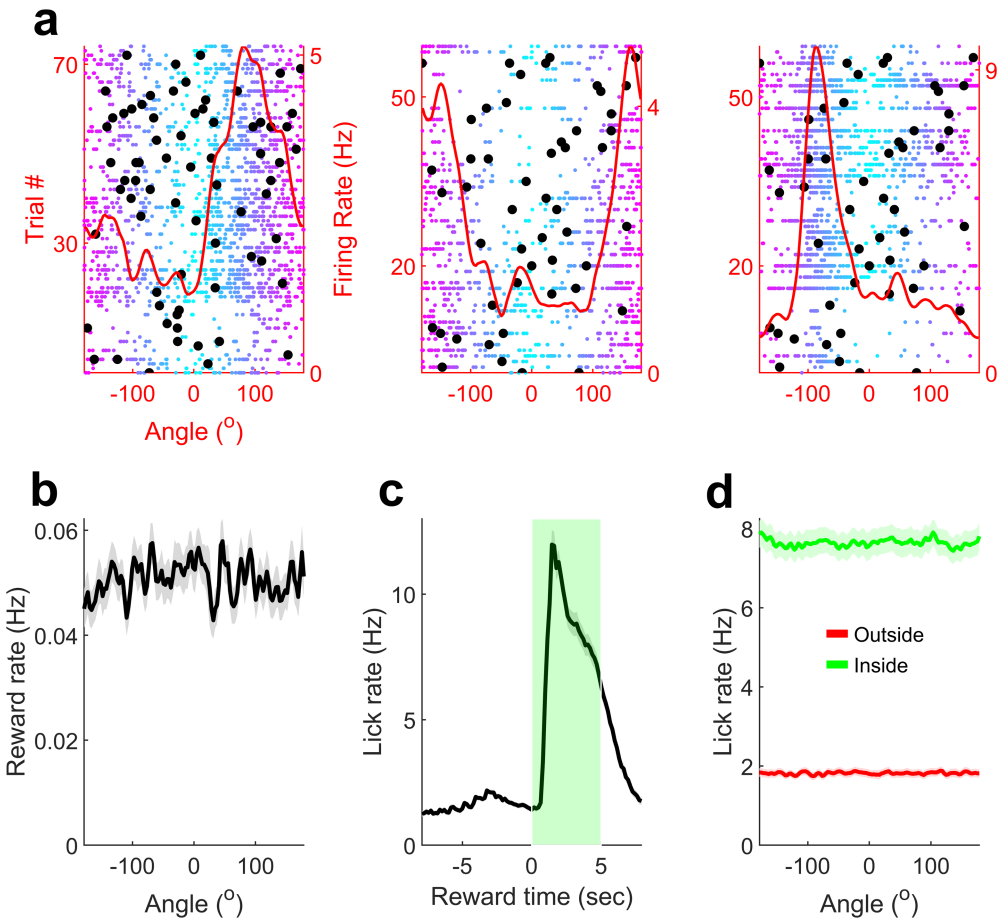
Extended Data Fig. 11 | Additional properties of aVEVS invariance. **a**, (Row 1) For same cells recorded in response to the movement of a green striped and green checkered bars of light, mean firing rates during stationary epochs (running speed < 5 cm/sec), were significantly correlated (*Pearson's r* = 0.48 p = 2×10^{-5}). Preferred angles of aVEVS between the two stimulus patterns were also significantly correlated (circular correlation coefficient, r = 0.32 p = 5×10^{-3}). Solid red dots denote preferred angles of cells tuned (sparsity (z) > 2) in both conditions; gray dots are for cells with significant tuning in one of the conditions. (Row 2) Same as **a** (Row 1), but for responses to changes of stimulus color, green and blue. Firing rate (r = 0.45 p = 1×10^{-4}) & preferred angle (r = 0.36 p = 0.01) were correlated. (Row 3) Same as **a** (Row 1), but for changes to predictability of the stimulus, also called “random” vs “systematic”. Firing rate (r = 0.55 p = 2×10^{-13}) & preferred angle (r = 0.27 p = 0.01) were significantly correlated between systematic and random stimuli movement. (Row 4) Same as **a** (Row 1), but for responses recorded across 2 days. Firing rate (r = 0.28 p = 3.2×10^{-5}) & preferred angle (r = 0.22 p = 0.006) were correlated. **b**, Similar to Fig. 3, we computed the population remapping indices based on sparsity difference, preferred angle difference and peak value of cross correlation. The sparsity difference did not show a systematic pattern, but the other two metrics generally showed increasing remapping going from pattern (correlation = 0.68, angle difference = 30°) to color (correlation = 0.64, angle difference = 46.5°) to predictability (correlation = 0.55, angle difference = 66°) and across days (correlation = 0.63, angle difference = 66°). n indicates the

number of responses measured in both conditions for each comparison, similar to Fig. 3h. Thick line – median, box – sem. **c**, Percentage of tuned responses in the random stimulus experiments, showing comparable bidirectionality (10% here vs 13% for systematically moving bar). **d**, For same cells recorded in random and systematic stimulus experiments, the distributions of firing rates and selectivity, quantified by z-scored sparsity, were not significantly different (cyan-systematic, purple-random, KS-test for z-scored sparsity p = 0.14, for firing rate p = 0.27). **e**, Cross correlation between CCW and CW tuning curves showing lagged response for the majority of bidirectional cells in the random condition. **f**, Same as **e**, but for unidirectional cells. **g**, Cross correlation of tuning curves (for tuned cells in the random stimulus experiment) between fast- and slow-moving stimulus was calculated from the subsample of data for a particular speed in CW and CCW direction separately and stacked together after flipping the CCW data and was not significantly biased from zero (Circular median test at 0°, p = 0.56). **h**, Example cell showing similar aVEVS for data within 1 s of stimulus direction change (top), or an equivalent, late subsample (bottom). **i**, Firing rate (KS-test p = 0.73) and sparsity (KS-test p = 0.87) were not significantly different for these two subsamples of experimental recordings. **j**, In the randomly moving stimulus experiments, we computed a stimulus speed modulation index (see Methods). This distribution was not significantly biased away from zero. **k**, This modulation index was z-scored (see Methods), and only 5.2% of cells had significant firing rate modulation beyond z of ± 2 .



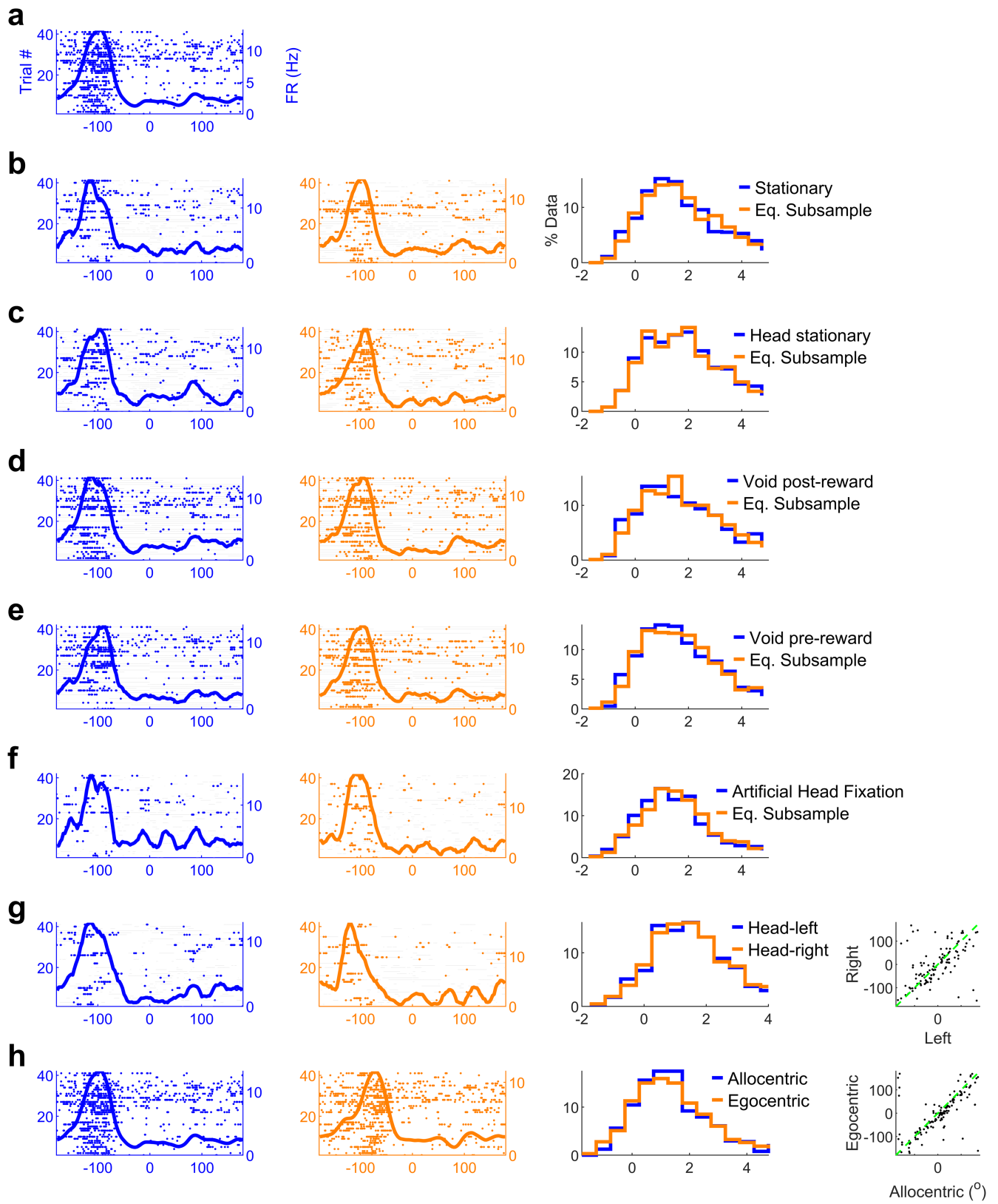
Extended Data Fig. 12 | Relationship between place cells, stimulus angle and distance (dVEVS) tuned cells. **a**, The mean firing rates of cells was significantly correlated ($Pearson's r = 0.43 p = 4.5 \times 10^{-10}$) between the aVEVS and place cell (spatial exploration) experiments. **b**, Majority of cells active during the aVEVS experiments were also active during random foraging in real world. **c**, Almost all of the aVEVS cells were also spatially selective during spatial exploration. **d**, Between the approaching and receding directions, the mean firing rates, computed when the rats were immobile, were highly correlated ($Pearson's r = 0.96 p = 4 \times 10^{-81}$) and not significantly different (KS-test $p = 0.99$). **e**, Firing rates, computed when rats were stationary, during the stimulus angle and stimulus distance experiments were significantly correlated ($r = 0.22 p = 0.008$). **f**, Population vector decoding of the stimulus distance (similar to stimulus angle decoding, Fig. 2), was significantly better than chance. (KS-test $p = 5.5 \times 10^{-10}$ for approaching and $p = 4.7 \times 10^{-9}$ for receding data). Approaching

stimulus decoding error (median = 194 cm) was significantly lesser than that for receding (median = 237 cm) (KS-test $p = 4.2 \times 10^{-5}$). These errors were 59% and 82% of the error expected from shuffled data, which was greater than that for aVEVS decoding, where the error was 33% of the shuffles, when controlling for the number of cells. **g**, More than twice as many cells were unidirectional tuned for approaching (coming closer) movement direction, as compared to receding (moving away). **h**, For bidirectional cells, location of peak firing in the approaching and receding direction shows bimodal response, with most cells preferring either the locations close to the rat, i.e., 0 cm or far away, ~500 cm. Unidirectional cells preferred locations close to the rat. **i**, Population vector overlap (Fig. 4j), was further quantified by comparing the values along the diagonal for actual tuning curves, with the spike train shuffles. The actual overlap was significantly above two standard deviations of the shuffles for distances close to the rat (around 0) and far away (beyond 400 cm).



Extended Data Fig. 13 | Rewards and reward related licking are uncorrelated with VEVS. **a**, Example cells showing aVEVS from Fig. 1, with reward times overlaid (black dots), showing random reward dispensing at all stimulus angles. **b**, The average rate of rewards was uncorrelated with visual stimulus angle (circular test for uniformity $p = 0.99$). **c**, Rat's consumption of rewards, estimated by the reward tube lick rate, was measured by an infrared

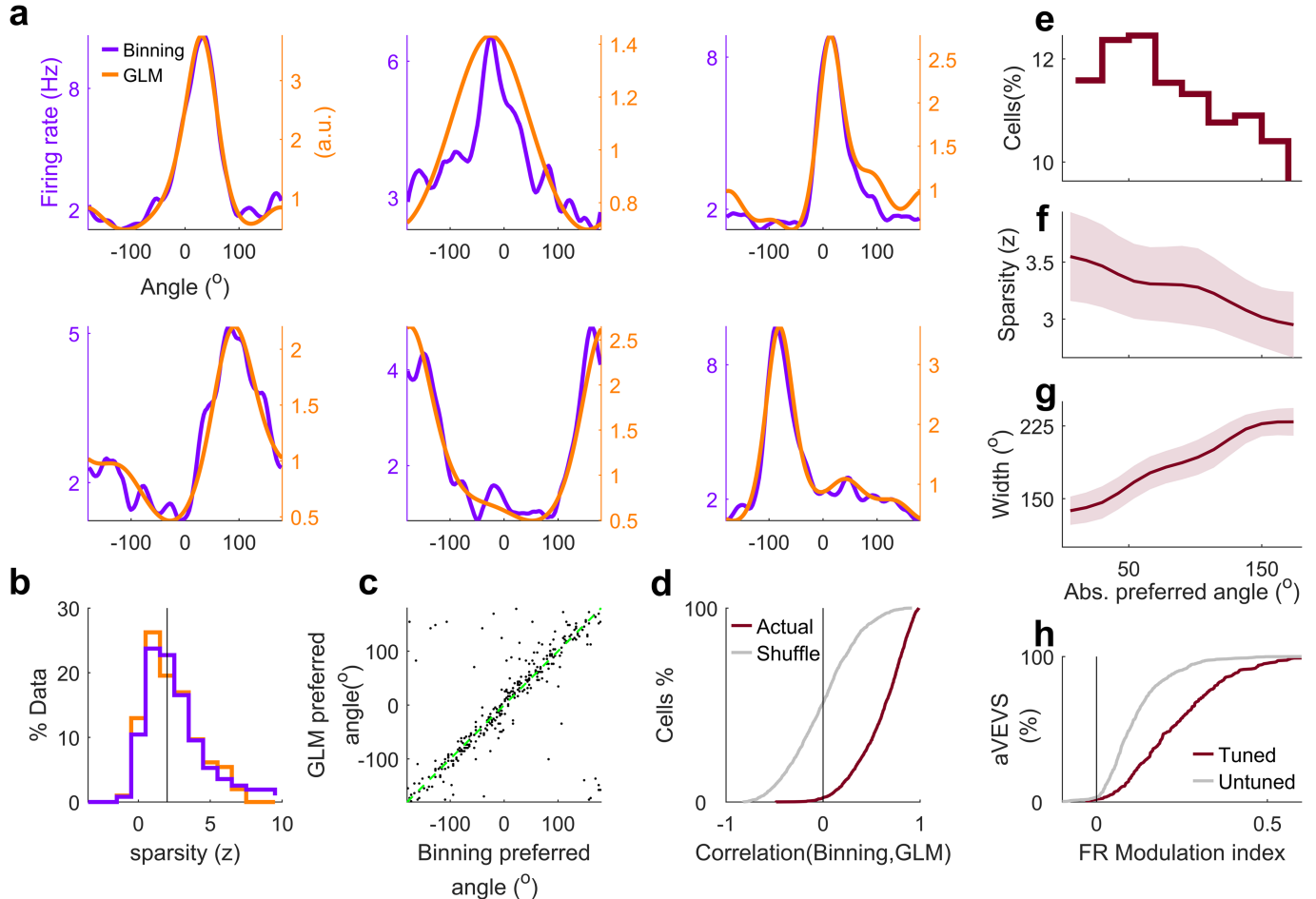
detector attached to the reward tube²⁶. As expected, lick rate increased after reward delivery by ~4 fold and remained high for about five seconds (green shaded area). This duration is termed the “reward zone”. **d**, Lick rate inside the reward zone (green) was significantly larger than that outside (red, KS-test $p = 2.3 \times 10^{-54}$). Inside as well as outside reward-zone lick rates were uncorrelated with visual stimulus angle (circular test for uniformity $p = 0.99$ for both).



Extended Data Fig. 14 | See next page for caption.

Article

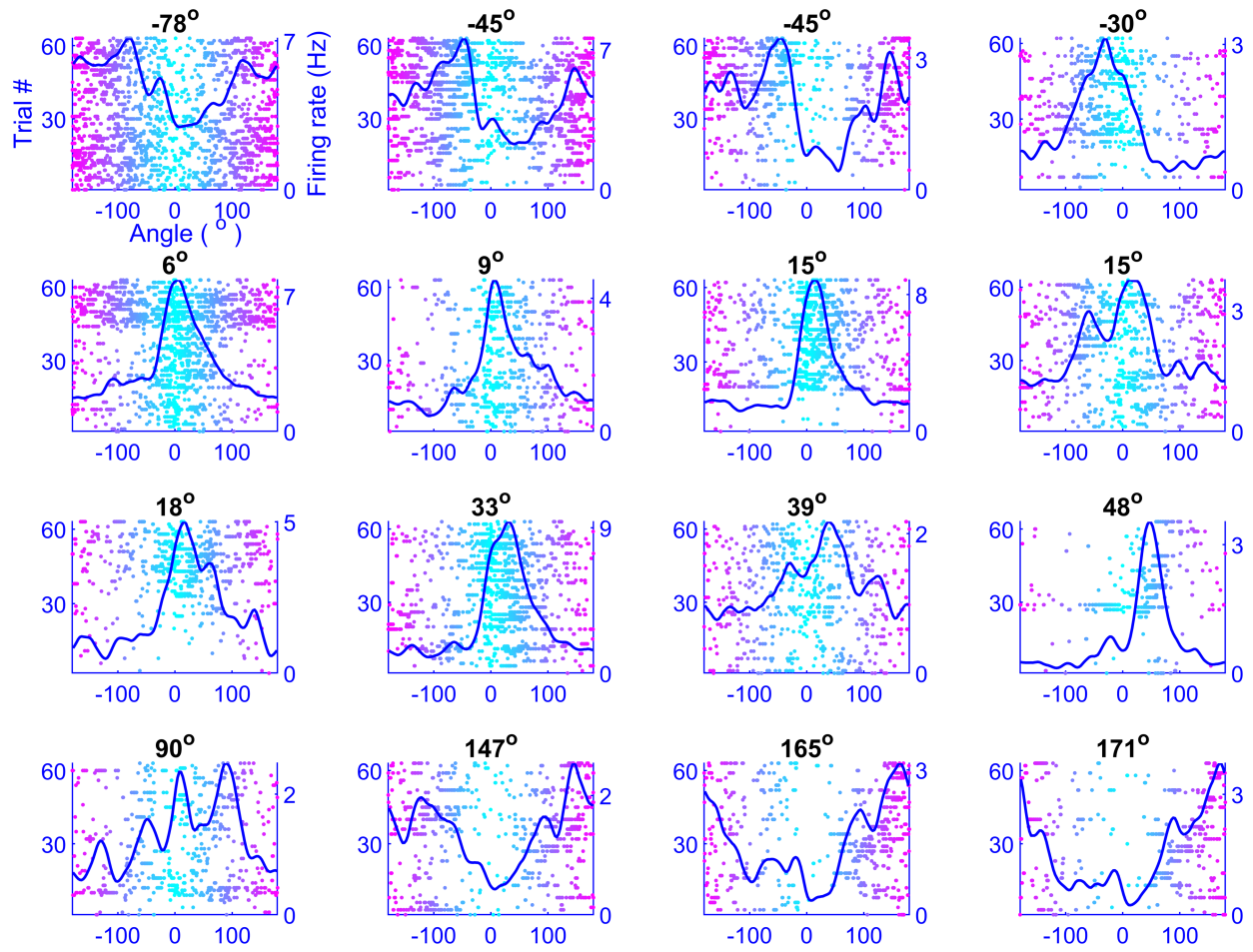
Extended Data Fig. 14 | Behavioral controls of VEVS. To ascertain whether systematic changes in behavior caused VEVS, we employed a ‘behavioral clamp’ approach and estimated tuning strength using only the subset of data where the hypothesized behavioral variable was held constant. **a**, Example aVEVS tuned cells maintained its tuning even if we used only the data when the rat was (**b**) stationary (running speed <5 cm/sec, blue, left). This was comparable to a random subsample of behavior, obtained by shuffling the indices of spikes and behavior when the animal was stationary (orange, middle) (see Methods). 38% of cells were aVEVS tuned (sparsity $z > 2$) when using only the stationary data which is significantly greater than chance, whereas 42% were significantly tuned in the equivalent, random subsample and this difference was significant (KS-test $p = 0.02$). **c**, Similar to **b** but using only the data when the rat’s head was immobile (head movement velocity <10 mm/sec). 43% and 42% of cells were significant tuned in actual behavioral clamp and equivalent subsample, and these were not significantly different (KS-test $p = 0.93$). **d**, Similar to **b**, but removing data within 5 s after reward dispensing, called void post-reward. 43% cells were tuned in “void post-reward” data, 43% for equivalent subsample (KS-test $p = 0.56$). **e**, Similar to **d**, but removing data within 5 s before reward dispensing, called void pre-reward. 39% cells were tuned for void pre-reward, 42% for equivalent subsample (KS-test $p = 0.43$). **f**, Using a subsample of data, from when the rat’s head was within the central 20 percentile of head positions (typically <10°), rat was stationary and there were no rewards in the last 5 s. This condition was called “analytical head fixation”. 28% of cells were aVEVS tuned under this behavioral clamp, which was lesser than that in an equivalent subsample (31%, KS-test $p = 0.05$), but significantly greater than chance. **g**, Tuning curves for head positions to the leftmost 20 percentile and rightmost 20 percentile were similar, with 31% and 32% cells tuned in the two conditions (KS-test $p = 0.67$). The preferred angles of tuning were highly correlated (circular correlation $r = 0.67 p = 1.3 \times 10^{-11}$) and not significantly different (circular KS-test $p > 0.1$). **h**, aVEVS tuning was recomputed in the head centric frame, by accounting for the rat’s head movements (obtained by tracking overhead LEDs attached to the cranial implant) and obtaining a relative stimulus angle, with respect to the body centric head angle. Overall tuning levels were comparable, between allocentric and this head centric estimation. First panel of **h** is the same as that in **a** since all aVEVS tuning reported earlier was in the allocentric or body centric frame. Using a subset of data when both overhead LEDs were reliably detected, 25% and 26% of cells were significantly tuned for the stimulus angle in the allocentric and egocentric frames (KS-test $p = 0.9$). Preferred angle of aVEVS tuning for tuned cells was highly correlated ($r = 0.81 p = 1.8 \times 10^{-15}$) and not significantly different between the two frames (circular KS-test $p > 0.1$).



Extended Data Fig. 15 | GLM estimate of aVEVS tuning. To estimate the independent contribution of stimulus angle to neural activity, while factoring out the contribution of head position and running speed, we used the generalized linear model (GLM) technique (see Methods)³⁰. **a**, Tuning curves obtained by binning methods were comparable with those from GLM estimation, including for the cells used in Fig. 1 (first 2 examples in row 1 & 2). **b**, Sparsity levels were comparable (KS-test $p = 0.07$) and 40% of cells were found to be significantly tuned for stimulus angle using GLM based estimates, compared to 43% from binning in this subset of data where head and leg movements were reliably captured (cell count, $n = 991$). **c**, Preferred angle of firing between GLM and binning based estimates of aVEVS were highly correlated (circular correlation test $r = 0.86 p < 10^{-150}$). **d**, Correlation between the aVEVS tuning curves from the two methods was significantly greater than

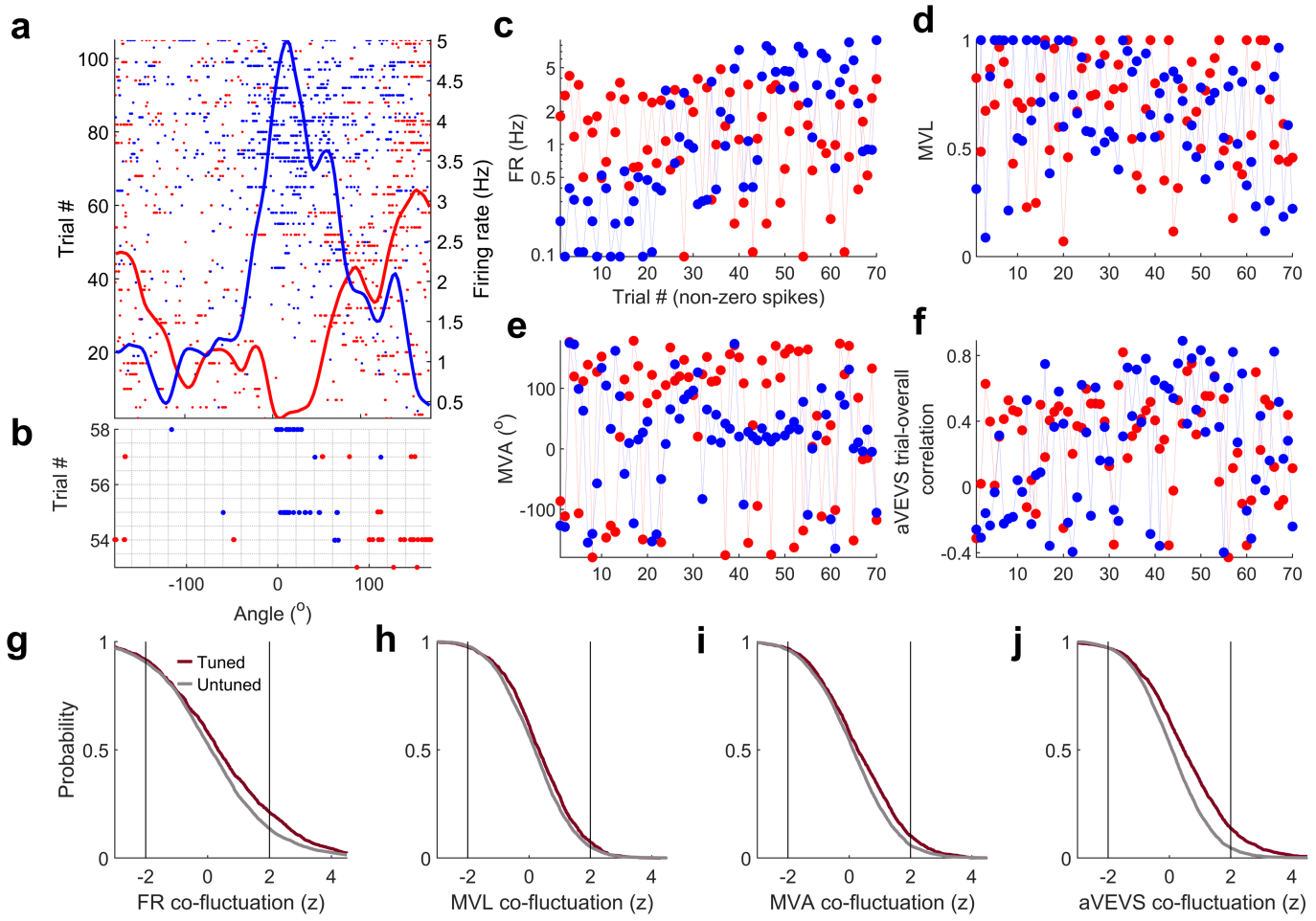
that expected by chance, computed by randomly shuffling the pairing of cell ID across binning and GLM (KS-test $p < 10^{-150}$). **e–h**, Properties of aVEVS tuning responses based on GLM estimates were similar to those based on binning method, as shown in Fig. 1. **e**, Distribution of tuned cells as a function of the preferred angle (angle of maximal firing). There were more tuned cells at forward angles than behind. **f**, Median \pm SEM z-scored sparsity and its variability (SEM, shaded area, here and subsequently) of tuned cells as a function of their preferred angle. (Pearson's $r = -0.17 p = 0.004$). **g**, Median \pm SEM full width at quarter maxima across the ensemble of tuned responses increased as a function of preferred angle of tuning. (Pearson's $r = +0.33 p < 10^{-150}$). **h**, CDF of firing rate modulation index within versus outside the preferred zone (see Methods) for tuned cells were significantly different (Two-sample KS test $p = 2.9 \times 10^{-37}$).

Article



Extended Data Fig. 16 | Simultaneously recoded cells span all angles.
16 simultaneously recorded cells showed significant aVEVS. Their preferred angles are indicated on top. Only cells selective for CCW direction shown for

clarity. While the forward direction (0°) is overrepresented, these cells span all angles of the visual field including angles behind him (180°).



Extended Data Fig. 17 | Simultaneously recorded cells show very weak co-fluctuation of aVEVS tuning across trials. **a, b.** Two simultaneously recorded cells showing significant aVEVS in the CCW direction (**a**), and zoomed in for a subset of trials, showing mostly uncorrelated fluctuations in the two cells' spiking (**b**). **c.** For the same cell-pair, mean firing rate across trials was broadly uncorrelated. Only trials with non-zero spikes were used here, and henceforth, to ensure comparison with aVEVS tuning (see below). **d.** Same as **c** but showing uncorrelated fluctuations in the depth of modulation of aVEVS response of the two cells across trials, quantified by the Mean Vector Length (MVL, see Methods). **e.** Same as **c** but showing uncorrelated fluctuation of aVEVS response across trials, quantified by Mean Vector Angles (MVA, see Methods). **f.** Same as **c** but showing largely independent fluctuations in the overall aVEVS tuning (measured by correlation between the trial-averaged aVEVS tuning curve and the aVEVS tuning curve in a given trial) for this cell-pair. The significance of co-fluctuations in cell-pairs were quantified by

bootstrapping methods, by employing trial id shuffles (see Methods). CCW and CW tuning curves were treated as separate responses throughout these analyses. **g.** 21% (14%) of simultaneously recorded, tuned (untuned) cell-pairs showed significant ($z > 2$) co-fluctuation of mean firing rates across trials which provides an estimate of the non-specific effects such as running, reward consumption etc. **h.** Only 7% (5%) of tuned (untuned) cell pairs showed significant co-fluctuation of MVL across trials indicating little effect of nonspecific variables on the depth of aVEVS tuning. **i.** Similarly, only 10% (6%) of tuned (untuned) cell pairs showed significant co-fluctuation of MVA across trials. **j.** Only 14% (5%) of tuned (untuned) cell pairs showed significant co-fluctuation of aVEVS. Notably, the number of cell pairs showing significant co-fluctuations in any of the aVEVS tuning properties (**h–j**) was smaller than the number of cell pairs showing significant co-fluctuation of firing rates; and there was little qualitative difference between the significantly aVEVS tuned vs untuned populations.

Reporting Summary

Nature Portfolio wishes to improve the reproducibility of the work that we publish. This form provides structure for consistency and transparency in reporting. For further information on Nature Portfolio policies, see our [Editorial Policies](#) and the [Editorial Policy Checklist](#).

Statistics

For all statistical analyses, confirm that the following items are present in the figure legend, table legend, main text, or Methods section.

n/a Confirmed

- The exact sample size (n) for each experimental group/condition, given as a discrete number and unit of measurement
- A statement on whether measurements were taken from distinct samples or whether the same sample was measured repeatedly
- The statistical test(s) used AND whether they are one- or two-sided
 - Only common tests should be described solely by name; describe more complex techniques in the Methods section.*
- A description of all covariates tested
- A description of any assumptions or corrections, such as tests of normality and adjustment for multiple comparisons
- A full description of the statistical parameters including central tendency (e.g. means) or other basic estimates (e.g. regression coefficient) AND variation (e.g. standard deviation) or associated estimates of uncertainty (e.g. confidence intervals)
- For null hypothesis testing, the test statistic (e.g. F , t , r) with confidence intervals, effect sizes, degrees of freedom and P value noted
 - Give P values as exact values whenever suitable.*
- For Bayesian analysis, information on the choice of priors and Markov chain Monte Carlo settings
- For hierarchical and complex designs, identification of the appropriate level for tests and full reporting of outcomes
- Estimates of effect sizes (e.g. Cohen's d , Pearson's r), indicating how they were calculated

Our web collection on [statistics for biologists](#) contains articles on many of the points above.

Software and code

Policy information about [availability of computer code](#)

Data collection	Electrophysiological data was collected using a Neuralynx acquisition system using Cheetah software. Control and rendering of the virtual reality environment was done with custom-written code in C++.
Data analysis	Spike sorting was done manually using custom software written in Python. All subsequent analyses were done using custom written scripts in MATLAB and using Circular Statistics Toolbox

For manuscripts utilizing custom algorithms or software that are central to the research but not yet described in published literature, software must be made available to editors and reviewers. We strongly encourage code deposition in a community repository (e.g. GitHub). See the Nature Portfolio [guidelines for submitting code & software](#) for further information.

Data

Policy information about [availability of data](#)

All manuscripts must include a [data availability statement](#). This statement should provide the following information, where applicable:

- Accession codes, unique identifiers, or web links for publicly available datasets
- A description of any restrictions on data availability
- For clinical datasets or third party data, please ensure that the statement adheres to our [policy](#)

The datasets generated during and/or analyzed during the current study are available from the corresponding author on reasonable request.

Field-specific reporting

Please select the one below that is the best fit for your research. If you are not sure, read the appropriate sections before making your selection.

- Life sciences Behavioural & social sciences Ecological, evolutionary & environmental sciences

For a reference copy of the document with all sections, see nature.com/documents/nr-reporting-summary-flat.pdf

Life sciences study design

All studies must disclose on these points even when the disclosure is negative.

Sample size	Eight Long Evans rats were used in the study with total 149 sessions in which 1191 well isolated, active pyramidal units were identified
Data exclusions	Single units with firing rates below 0.2Hz were excluded. This is typical in the field.
Replication	Stimulus angle and distance selective neurons were found in all subjects.
Randomization	Randomization was not necessary as multiple groups were not being compared.
Blinding	Blinding is not relevant to our study, since all subjects were subjected to the same experiments, and the further analyses were blind to the subject source of the data.

Reporting for specific materials, systems and methods

We require information from authors about some types of materials, experimental systems and methods used in many studies. Here, indicate whether each material, system or method listed is relevant to your study. If you are not sure if a list item applies to your research, read the appropriate section before selecting a response.

Materials & experimental systems		Methods	
n/a	Involved in the study	n/a	Involved in the study
<input checked="" type="checkbox"/>	<input type="checkbox"/> Antibodies	<input checked="" type="checkbox"/>	<input type="checkbox"/> ChIP-seq
<input checked="" type="checkbox"/>	<input type="checkbox"/> Eukaryotic cell lines	<input checked="" type="checkbox"/>	<input type="checkbox"/> Flow cytometry
<input checked="" type="checkbox"/>	<input type="checkbox"/> Palaeontology and archaeology	<input checked="" type="checkbox"/>	<input type="checkbox"/> MRI-based neuroimaging
<input type="checkbox"/>	<input checked="" type="checkbox"/> Animals and other organisms		
<input checked="" type="checkbox"/>	<input type="checkbox"/> Human research participants		
<input checked="" type="checkbox"/>	<input type="checkbox"/> Clinical data		
<input checked="" type="checkbox"/>	<input type="checkbox"/> Dual use research of concern		

Animals and other organisms

Policy information about [studies involving animals](#); [ARRIVE guidelines](#) recommended for reporting animal research

Laboratory animals	Eight adult male Long-Evans rats were used in the study, and were 3 months old at the start of experiments.
Wild animals	Wild animals were not used in our study
Field-collected samples	No field collected samples were used in our study
Ethics oversight	All experimental procedures were approved by the UCLA Chancellor's Animal Research Committee and were conducted in accordance with USA federal guidelines.

Note that full information on the approval of the study protocol must also be provided in the manuscript.